



On the causes of tropical cyclone driven floods in India

Akshay Rajeev^a, Vimal Mishra^{a,b,*}

^a Earth Sciences, Indian Institute of Technology IIT, Gandhinagar, India

^b Civil Engineering, Indian Institute of Technology IIT, Gandhinagar, India

ABSTRACT

Landfalling tropical cyclones (TCs) cause severe damage to infrastructure and economic losses in India. Extreme rainfall from TCs can lead to flooding, which disrupts the lives of people and their socio-economic well-being. Despite the severe hazards caused by TCs in India, their impacts on river basin-scale flooding are not well examined. Here, we use cyclone tracks from India Meteorological Department (IMD) and ERA5-Land reanalysis to identify the drivers of TC induced floods in India. We select TCs that affected the Subarnarekha, Brahmani, Mahanadi, and Vamshadhar river basins during the 1981–2019 period. We estimated return periods of extreme daily and hourly rainfall and total runoff associated with TCs. We examined the role of antecedent soil moisture on floods caused by TCs. Our results show that the distribution of extreme rainfall over a basin from TCs depend on the translation speed, track length, and size of the TC. Severe flooding in the basins is strongly linked to antecedent soil moisture conditions. Regardless of extreme rainfall, flooding due to TCs during the pre-monsoon (April–May) is less likely because of dry antecedent soil moisture conditions. On the other hand, TCs can lead to severe flooding during the summer monsoon (June–September) period due to relatively wetter antecedent conditions. In the post-monsoon season (October–November), the severity of flooding caused by TCs is higher than the pre-monsoon season, and as we move further into the post-monsoon this severity reduces. Our findings highlight the need to monitor the land-surface characteristics and TC track prediction to identify the potential of flooding from landfalling TCs.

1. Introduction

Tropical cyclones (TCs) are intense circular storms that originate over tropical oceans and are among the most significant threats to human life and property in the world (WMO, 2020). TCs are associated with heavy rainfall and strong winds, which cause hazards such as storm surges and inland flooding. The Indian subcontinent is adversely affected due to its long coastline exposed to most of the TCs originating in the north Indian Ocean (National Disaster Management Authority, 2008). Most of the TCs originate from over the Bay of Bengal, which affects the eastern coast of India. Despite having a smaller area compared to other TC basins, the Bay of Bengal produces 5% of the world's TCs (Hoarau et al., 2012). The shallow bathymetry and coastal terrain, and a high population density along the rim of the Bay of Bengal lead to devastating consequences. For instance, about 80% of the world's fatalities due to TCs are caused by TCs originating from the Bay of Bengal (Needham et al., 2015). Since the Bay of Bengal is surrounded by land, most of the TCs that originate here make landfall (Balaguru et al., 2014).

Compared to other regions, the north Indian Ocean produces fewer TCs. However, the annual TC formation here shows a bimodal pattern, with one peak during the pre-monsoon (April–May) and the other during the post-monsoon [October–November] (Evan and Camargo, 2011;

Gray, 1968; Li et al., 2013). The frequency of TC formation in the north Indian Ocean is higher during the post-monsoon; however, the TCs that form during the pre-monsoon period have greater intensities (Li et al., 2013). The bimodal pattern is mainly due to the weak vertical wind shear during the pre-and post-monsoon and its strengthening during the monsoon period (Hoarau et al., 2012; Li et al., 2013; Xing and Huang, 2013). Various studies show that the El Nino Southern Oscillations (ENSO) and the Indian Ocean Dipole (IOD) strongly influence the frequency, intensity, and location of origin of TCs in the Bay of Bengal (Bhardwaj et al., 2019; Girishkumar and Ravichandran, 2012; Mahala et al., 2015).

Two major hazards associated with TCs are coastal flooding, which depends on rainfall and storm surge, and inland flooding that mainly depends on rainfall accumulations. The total rainfall over a region due to a TC primarily depends on its translation speed and rainfall area (Rogers et al., 2009; Titley et al., 2021). Various studies based on the observations and numerical modelling demonstrate an increase in the rainfall rate associated with TCs due to climate change, suggesting a rise in flood risk associated with TC events (Knutson et al., 2015; Patricola and Wehner, 2018; Risser and Wehner, 2017). Even though multiple studies concentrate on the various aspects of cyclone activity (such as genesis, intensity, and track forecast) in the north Indian Ocean (Balaguru et al., 2014; Sahoo and Bhaskaran, 2015; Singh et al., 2000; Srinivas et al.,

* Corresponding author. Earth Sciences, Indian Institute of Technology IIT, Gandhinagar, India.

E-mail address: vmishra@iitgn.ac.in (V. Mishra).

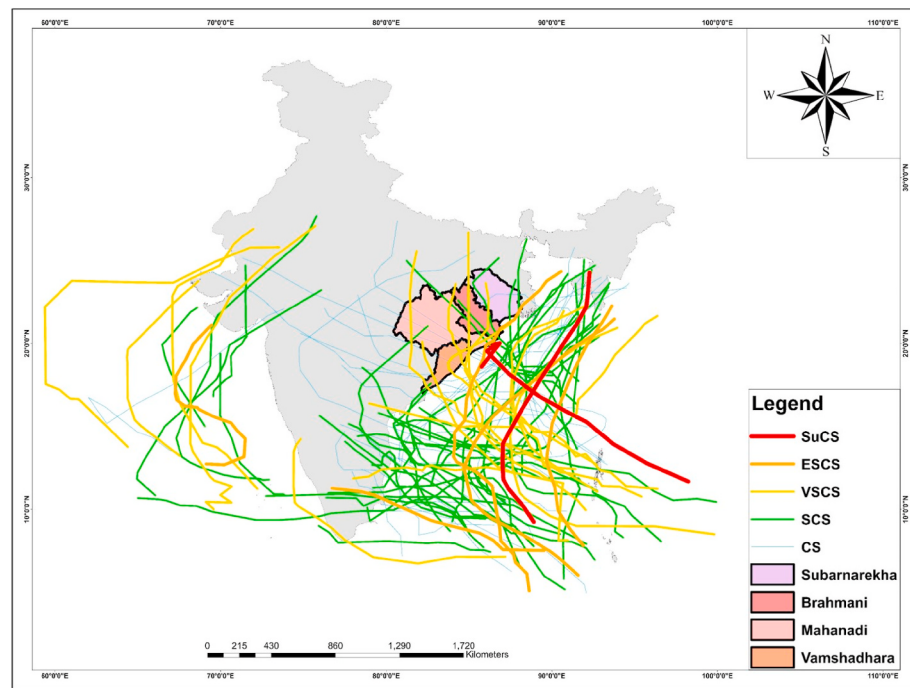


Fig. 1. Map showing tracks of TCs which affected Indian region from 1981 to 2019. The four basins considered in this study are also highlighted above using different colours. The different colours and the thickness of the tracks represent the maximum intensity of the TC where the red track represents Super Cyclonic Storms (SuCS), the orange track represents Extremely Severe Cyclonic Storms (ESCS), the yellow track represents Very Severe Cyclonic Storms (VSCS), the green track represents Severe Cyclonic Storms (SCS) and the blue track represents Cyclonic Storms (CS). (For interpretation of the references to colour in this figure legend, the reader is referred to the Web version of this article.)

2013), the majority of the work related to TC induced flooding focus on coastal vulnerability and damage assessment (Hoque et al., 2018; Rao et al., 2015; Sahoo and Bhaskaran, 2018). However, efforts to quantify the impact of TCs on flooding in river basins have remained elusive mainly because of the complex spatio-temporal variability of flood processes associated with rainfall and the basin characteristics such as regional topography and soil moisture conditions (Houze, 2012; Smith et al., 2005; Woods and Sivapalan, 1999). Recent work by Titley et al. (2021) investigated the relationship between TC precipitation and riverine flood. It demonstrated that flood intensity is not strongly correlated with TC intensity, showing a need to reassess the risk associated with TCs.

Currently, the TC warning provided in India is based primarily on the wind hazard associated with each event (Mohapatra et al., 2014). However, it is necessary to understand the flood risk related to each TC event in each season to minimize the social and economic losses by landfalling TCs. The primary goal of the present study is to examine the role of land surface conditions on flooding in Indian river basins due to landfalling TCs. The scientific questions that we aim to address are: i) Do TCs cause flooding in Indian river basins?, ii) How does the spatio-temporal distribution of extreme rainfall caused by TCs affect flooding?, and iii) What is the role of antecedent soil moisture in generating floods over the Indian river basins? To answer these questions, we use the TC tracks provided by the India Meteorological Department (IMD) to extract the dates and tracks of TCs impacting the Indian region. We also examine the performance of ERA5-Land precipitation and runoff over the Indian river basins. Finally, we investigate the potential of TC induced flooding in the Indian river basins during different periods based on the return period of rainfall and floods in relation to the antecedent soil moisture in the basins.

2. Data and methods

2.1. Cyclone tracks

Four major Indian river basins were selected, which are located along the eastern coast of India that is most affected by TCs (Fig. 1). The cyclone tracks of the TCs used in this study were obtained from the Cyclone eAtlas of IMD. The Cyclone eAtlas – IMD is an electronic atlas of

cyclonic disturbances (CD) over the North Indian Ocean from 1891 to the present year (Cyclone eAtlas-IMD, 2021). The atlas provides cyclone tracks of three categories Depression (D) [31–51 km/h], Cyclonic Storm (CS), and Severe Cyclonic Storm (SCS), with daily TC location, classified based on their maximum intensity. The SCS category has been further divided into various categories based on sustained wind speeds. Fig. 1 shows the cyclone tracks over the Indian region categorized into Cyclonic Storm (CS) [62–87 km/h], Severe Cyclonic Storm (Severe Cyclonic Storm) [88–117 km/h], Very Severe Cyclonic Storm (VSCS) [118–165 km/h], Extremely Severe Cyclonic Storm (ESCS) [166–221 km/h], and Super Cyclonic Storm (SuCS) [≥ 221 km/h] based on the Tropical Cyclone classification of IMD (IMD, 2021). The detailed report of each cyclonic disturbance in the North Indian Ocean since 1990, published by the Regional Specialized Meteorological Centre were also used for details about each TC event (RSMC, 2020). We only consider cyclonic disturbances belonging to CS or the higher categories covering 1981 to 2019 and passing over the river basins under investigation (Fig. 1).

2.2. Precipitation, runoff and soil moisture

Daily gridded precipitation data at a resolution of 0.25° were obtained from the Indian Meteorological Department for 1981 to 2019. The gridded precipitation is developed using more than 6500 gauge stations across India (Pai et al., 2014) using the Inverse Distance Weighted Interpolation (IDW) Technique (Shepard, 1968). Compared with other observational datasets, the gridded precipitation exhibited good similarities of the large-scale climatological features in the annual and seasonal rainfall patterns (Pai et al., 2014). The location of the streamflow gauge stations and daily streamflow observations were obtained from India Water Resource and Information System (WRIS) for the four basins.

Since the aim is to understand the influence of TCs on flooding in the Indian river basins, the ERA5-Land reanalysis dataset was used as the coarser resolution of the IMD dataset may not be sufficient to study the TC rainfall affected area. Additionally, ERA5-Land provides hourly precipitation, whereas only daily observations are available from IMD. As TCs pass over a region in a short period, this increased temporal resolution is necessary to understand the distribution of TC rainfall at a

location. Hence, we obtain daily and hourly precipitation, total runoff, and volumetric soil moisture at 0.1° spatial resolution from the ERA5-Land reanalysis. ERA5-Land reanalysis data are developed by the Copernicus Climate Change Service (C3S) at European Centre for Medium-Range Weather Forecasts (ECMWF) and are available from 1981 to the present (Muñoz-Sabater et al., 2021). ERA5-Land is a high resolution, an improved version of the land component of the ERA5, and is based on the H-Tessel land surface model. The suitability of ERA5-Land data for hydrological applications in India has not been investigated. However, the performance of the ERA5 reanalysis dataset over the Indian region has shown that it is suitable for hydrological assessment in India (Mahto and Mishra, 2019). Hence, being an improved version of ERA5, ERA5-Land is also expected to perform well for hydrological applications over the Indian region. The availability of continuous data and the variety of variables with high resolution from ERA5-Land are vital for examining the role of land surface conditions on flooding during TCs.

2.3. RVIC routing model

The RVIC model is a modified version of the streamflow routing model associated with the post-processor with the Variable Infiltration Capacity (VIC) hydrology model. The RVIC is a source-to-sink model

which uses a linearized version of the Saint-Venant equations. This model, which utilizes Impulse Response Functions (i.e., Unit-Hydrographs) to represent the distribution of flow at the outlet point for the time from an impulse input at each source point, has been developed by Lohmann et al. (1996). The standalone routing model has been used in multiple studies at different spatial scales (Brunke et al., 2018; Hamlet et al., 2013; LOHMANN et al., 1998; Nijssen et al., 1997; Su et al., 2005). The primary input for this model is the surface runoff and baseflow. The hourly total runoff (surface runoff + baseflow) from the ERA5-Land is used as it consists of a surface and subsurface component. A 0.1° DEM (resampled from 90 m Shuttle Radar Topography Mission (SRTM) DEM) is used to generate each basin's impulse response function parameters. A detailed description of the RVIC model is available in Hamman et al. (2017) and <https://rvic.readthedocs.io>. In this study, the RVIC routing model is primarily used to route the total runoff to assess the performance of ERA5-Land against observed streamflow.

2.4. Methodology

The cyclone tracks were used to estimate the basins affected by each TC and to extract the dates when those made landfall. Following this, the most affected area of the basin by each TC event was estimated based on

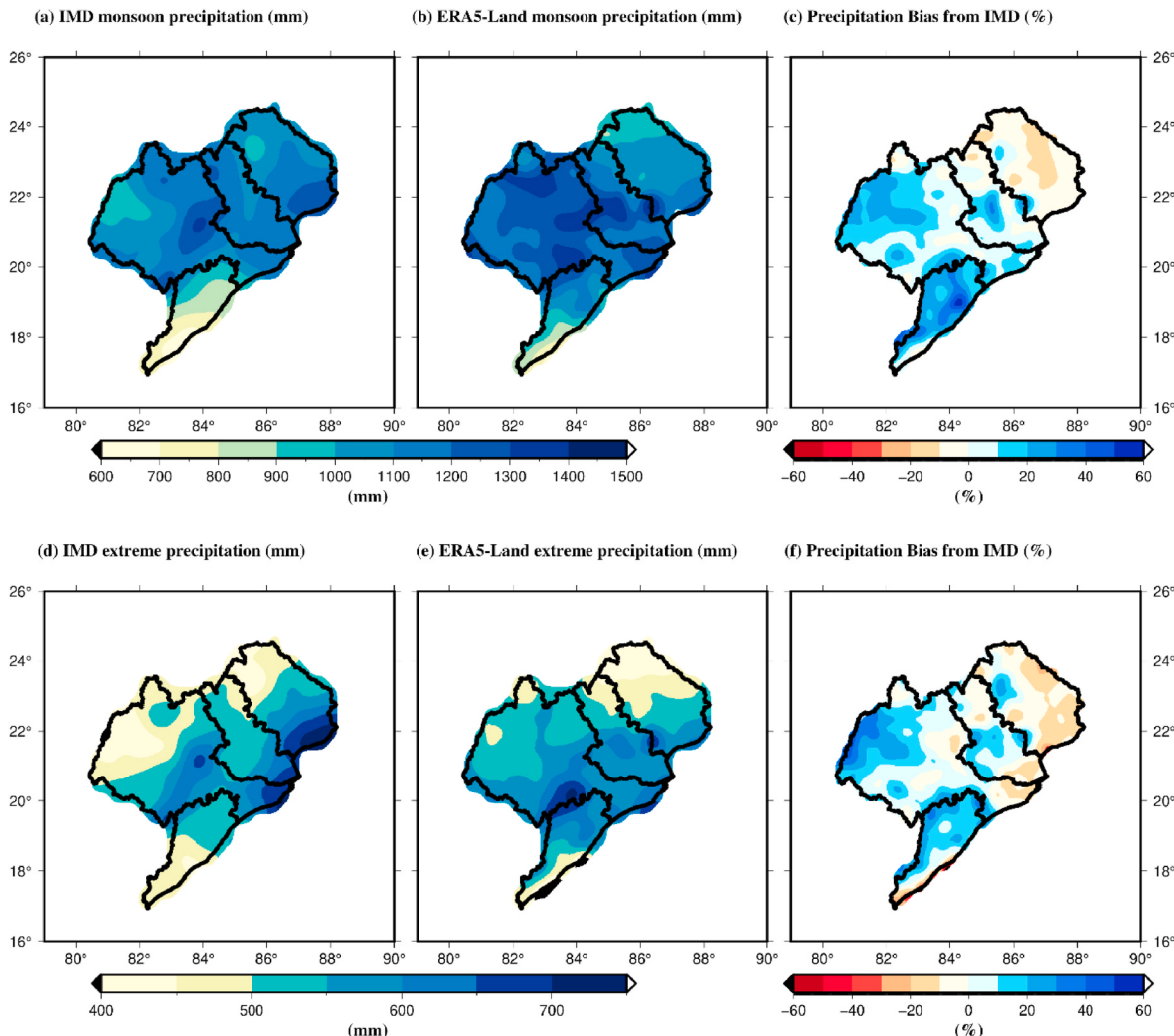


Fig. 2. Long-term observed monsoon season precipitation (mm) a) IMD, b) ERA5-Land and c) median bias (%) in the summer monsoon season (JJAS) precipitation 1981–2019 period over Subarnarekha, Brahmani, Mahanadi and Vamshadhabra. Long-term observed extreme precipitation (mm) d) IMD, e) ERA5-Land and f) median bias (%) in the extreme precipitation 1981–2019 period over Subarnarekha, Brahmani, Mahanadi and Vamshadhabra.

rainfall distribution. Here, the most affected region is defined in terms of TC rainfall accumulations and is the region of the basin with daily rainfall greater than 50 mm on the day the TC passes over the basin. In case a TC event remained over a region for more than one day, we consider only the day on which it received highest rainfall during the period. The daily and hourly rainfall/runoff values were then averaged over this region providing us with 36 rainfall/runoff events corresponding to the 36 TC events considered for the analysis. If an event passes over multiple basins, we consider the impact over each basin separately. For example, if a TC passes over two basins, then we get two separate time series for rainfall/runoff. The spatial average of this region is used instead of the basin average as some TC events may affect only a very small portion of the basin which can cause the underestimation of rainfall/runoff values if the entire basin was considered. The translation speed and track length of TCs were also estimated as it can have a strong impact on the rainfall during such events (Titley et al., 2021). Since the Cyclone eAtlas provides daily TC location along the track, the average translation speed was estimated from the entire length of the TC tracks and the time taken by TC to cover this path. We use the full length of the track as the translation speed reduces when a TC makes landfall and the average speed of the TC over the ocean is also important for moisture uptake.

To assess the performance of the ERA5-Land dataset over this region, the median bias of monsoon (June to September) season precipitation and extreme precipitation (90th Percentile precipitation) against IMD precipitation over the four river basins was estimated. The hourly total runoff from ERA5-Land was routed using the RVIC routing model to generate daily streamflow at each station location. The performance ERA5-Land derived daily streamflow was also assessed against observed daily streamflow where continuous observations are available using correlation Normalized Root Mean Square Error (NRMSE), bias, and Nash Sutcliffe Efficiency (Nash and Sutcliffe, 1970).

To assess the influence of landfalling TCs on flooding in Indian river basins, we used the daily and hourly precipitation and total runoff derived from ERA5-Land extracted for each TC event for all the basins. Since total runoff has a surface and sub-surface component, it is expected to be correlated with the streamflow. Hence, we use the total runoff as a proxy for streamflow, as the rainfall distribution of TCs is such that different TCs affect different gauge stations. Also, the gauge station may not capture the TC-induced flooding as the gauge station may be too far downstream from the area affected by TC. The rainfall and total runoff associated with each TC event used in the analysis is spatially averaged over the most affected region. We then compare the peak and mean daily precipitation during various TCs with the summer monsoon (June–September) period. Similarly, the daily runoff was also compared. The vertically integrated water vapour flux anomaly and wind (U and V) at 850 hPa with each event was estimated to determine the influence of TC size on rainfall over a region.

The return periods of daily and hourly rainfall were estimated for the parts of the basins affected by each TC event by fitting the annual maximum daily/hourly precipitation to the Generalized Extreme Value (GEV) curve. We tested various distributions and found GEV as the best-fit distribution based on negative log-likelihood (Tables S1 and S2). Correspondingly, the return periods of daily and hourly total runoff associated with each TC event was calculated by fitting annual maximum daily/hourly runoff values to the GEV distribution. Finally, the return periods of precipitation and total runoff were compared to assess the impact of TC rainfall on flooding in the basin. Please see supplemental information on the detailed method for return period estimation. Additionally, the volumetric soil water content of the top 60 cm was estimated by combining all four layers of the reanalysis dataset as this extends to the root zone (Mishra et al., 2018). The root-zone soil moisture is crucial in the water and energy cycles and influences flood generation (Paschalis et al., 2014). To understand the influence of basin conditions before a TC in causing floods, the seven-day soil moisture percentile was calculated. We converted volumetric water content of the

top 60 cm to soil moisture percentiles using the empirical cumulative distribution function at each grid. An empirical cumulative distribution function is built from the daily soil moisture measurements using a 7-day moving average centred on a target date. The 7-day moving average includes values from three days before the target date and three days after the target date for all the years. Percentiles are estimated from the empirical distribution generated from these data for the entire time period for all grids of a basin. We used 7-day soil moisture percentile corresponding to the 7 days prior to the landfall date of each TC.

3. Results

3.1. Performance evaluation of ERA5 land precipitation

First, we evaluated bias in ERA5-Land during the monsoon season precipitation for the 1981–2019 period against observed data from IMD for each of the four basins. The observed mean monsoon season precipitation for 1981–2019 in the four basins range between 636 mm and 1364 mm, with higher rainfall observed in the Mahanadi basin and lower rainfall along the coast of the Vamshadbara basin (Fig. 2a). Similarly, the ERA5-Land mean monsoon precipitation in the four basins range between 666 mm and 1704 mm with higher rainfall in the Mahanadi and Brahmani basin and lower precipitation in the Vamshadbara basin (Fig. 2b). For the summer monsoon period, the ERA5-Land shows a basin-wise median bias of −4.9%, 5.8%, 10.8%, 24% for Subarnarekha, Brahmani, Mahanadi and Vamshadbara basins, respectively (Fig. 2c). Thus, in three of the four basins, ERA5-Land overestimates monsoon season precipitation.

Next, we compared the bias in extreme precipitation in the ERA5 Land reanalysis during 1981–2019. For this comparison, the 90th percentile rainfall of rainy days (precipitation more than or equal to 1 mm) for the entire calendar year (Jan–Dec) was used. The observed extreme daily rainfall during 1981–2019 ranged between 425 mm and 760 mm (Fig. 2d). Extreme rainfall from ERA5 Land during this period ranged between 420 mm and 760 mm (Fig. 2e). For the extreme precipitation, ERA5-Land shows a basin wise median bias of −5.1%, 4.4%, 8.5% and 13.2% for Subarnarekha, Brahmani, Mahanadi and Vamshadbara basins, respectively (Fig. 2f). Thus, similar to the monsoon season precipitation, we find an overestimation in extreme rainfall in the ERA5-Land dataset in three of the four basins. The bias in precipitation over Vamshadbara basin is particularly high. This may be because a large portion of this basin has high elevation (Fig. S1) and ERA5-Land overestimates precipitation at higher elevations particularly between 500 m and 2000m (Chen et al., 2021). The overestimations in rainfall have also been observed in the ERA5 reanalysis dataset (Mahto and Mishra, 2019), from which ERA5-Land was developed. Additionally, it should be noted that the IMD dataset against which ERA5-Land data was assessed will also have errors based on the density and reliability of gauge stations as the dataset is interpolated from such gauge station data (Jena et al., 2020).

3.2. Performance evaluation of streamflow

To understand flooding in river basins during TC events, we used the total runoff from ERA5-Land as a proxy to streamflow. For this, the total runoff from ERA5-Land was routed using the RVIC routing model to generate streamflow at various locations in each basin where continuous streamflow observations are available (Fig. S1). The RVIC routing model can also be used to generate sub-daily streamflow. Since the performance evaluation is done against observed daily streamflow, the routed daily streamflow from ERA5-Land for 1981–2019 was used. We first compared the annual maximum simulated streamflow against the observed annual maximum streamflow for each basin to evaluate ERA5 Land's performance. The simulated and observed streamflow at most of the locations correlates moderately well with correlation coefficients of 0.57, 0.48, 0.79 and 0.58 for Jamshedpur, Gomlai, Basantpur and

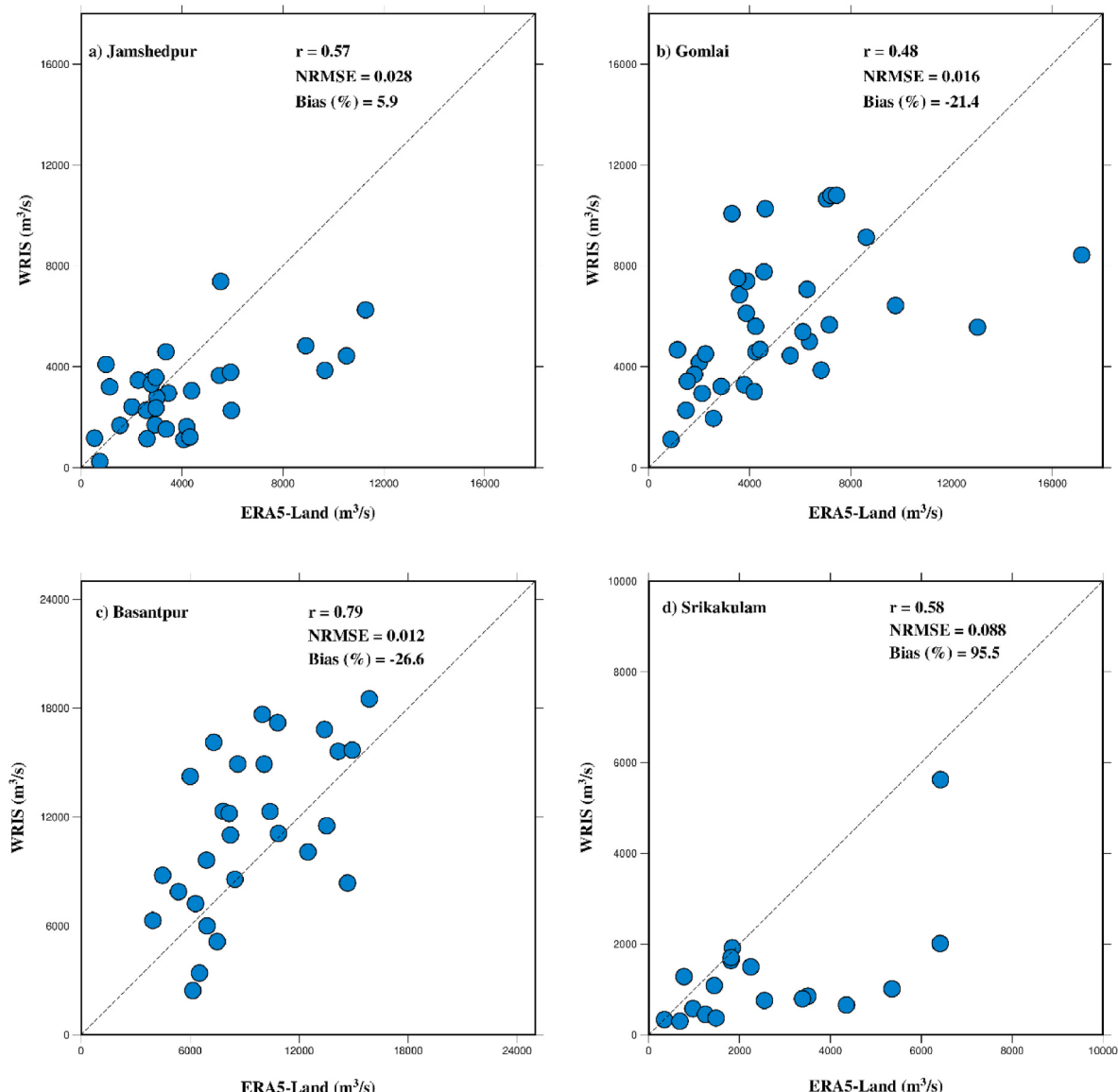


Fig. 3. Comparison of annual maximum daily streamflow of ERA5-Land and India-WRIS observations (a) Gomlai of Brahmani basin, (b) Basantpur of Mahanadi basin, (c) Jamshedpur of Subarnarekha basin, (d) Srikakulam of Vamshadhar basin.

Table 1

Correlation coefficients (r) and Nash Sutcliffe Efficiency (NSE) of ERA5-Land simulated daily streamflow against WRIS-Observation Streamflow. The Nash-Sutcliffe coefficient of Efficiency (NSE) (Nash and Sutcliffe, 1970) is a widely used indicator of the accuracy of model simulations. NSE values range between ∞ and 1. Here, 1 shows the perfect fit of simulated and observed data, and $NSE < 0$ indicates a poor fit.

Basin (Years)	Streamflow Station	r	NSE
Subarnarekha	Govindapur (1993–2012)	0.48	-0.28
	Jamshedpur (1981–2010)	0.50	0.02
Brahmani	Anantapur (1981–2000)	0.50	-0.01
	Gomlai (1981–2015)	0.57	0.26
Mahanadi	Basantpur (1981–2009)	0.58	0.30
	Kantamal (2001–2010)	0.51	0.03
Vamshadhar	Purushottampur (1999–2007)	0.29	-0.48
	Srikakulam (1991–2008)	0.54	-0.57

Srikakulam, respectively (Fig. 3). However, bias in streamflow across various basins shows significant variations with 5.9%, -21.4%, -26.6 and 95.5% for Jamshedpur, Gomlai, Basantpur and Srikakulam,

respectively.

We also compared daily streamflow simulation against observations at each of the stations where continuous data is available. The simulated streamflow had a moderate correlation with the observed streamflow at most stations (Table 1). Additionally, we estimated Nash Sutcliffe Efficiency (NSE) values that signify the ability of ERA5-Land in simulating extreme streamflow events. The simulated streamflow shows negative NSE values at Govindapur, Anantapur, Purushottampur and Srikakulam. Moreover, the NSE values at the remaining stations ranges between 0 and 0.3 which is below the ideal value of $NSE \geq 0.5$. This below-average performance based on NSE can be attributed to the overestimation of precipitation in ERA5-Land and directly affects the simulation of total runoff in the reanalysis dataset (Mahto and Mishra, 2019). Additionally, the use of a coarse resolution DEM from which the impulse response function parameters for each basin were generated may also have influenced the streamflow routing.

Table 2

Peak precipitation and runoff in the area affected by tropical cyclones during monsoon period (1981–2019) and TC events.

Basin	Date of TC event	Precipitation (mm)				Runoff (mm)			
		Daily Monsoon Peak	Hourly Monsoon Peak	Daily TC Peak	Hourly TC Peak	Daily Monsoon Peak	Hourly Monsoon Peak	Daily TC Peak	Hourly TC Peak
Subarnarekha	14-Oct-1985 to 18-Oct-1985	105.98	9.60	64.22	5.29	72.78	7.44	14.86	3.06
	23-May-1989 to 28-May-1989	141.94	16.41	147.57	15.16	83.32	14.75	49.84	8.66
	07-Nov-1995 to 11-Nov-1995	96.98	8.47	73.29	5.57	58.06	5.94	11.72	1.69
	15-Oct-1999 to 20-Oct-1999	145.18	12.77	96.89	8.63	57.59	7.84	34.38	6.09
	25-Oct-1999 to 31-Oct-1999	140.94	14.93	76.38	7.09	77.96	13.35	30.02	4.43
	31-Jul-2015 to 06-Aug-2015	115.17	10.95	63.61	5.20	36.07	6.17	30.69	3.34
	10-Oct-2018 to 16-Oct-2018	145.87	14.82	100.46	10.03	76.13	13.06	35.88	6.14
	01-May-2019 to 05-May-2019	129.70	10.58	107.53	9.26	47.43	6.37	21.95	3.40
	07-Nov-2019 to 12-Nov-2019	121.79	11.74	60.36	4.79	60.49	10.02	15.60	2.35
	14-Oct-1985 to 18-Oct-1985	217.06	17.46	98.88	8.49	139.16	16.74	46.33	6.41
Brahmani	23-May-1989 to 28-May-1989	171.04	17.54	79.61	9.00	151.51	12.88	22.04	4.26
	15-Oct-1999 to 20-Oct-1999	115.26	12.99	75.10	7.14	55.34	14.72	23.78	3.47
	25-Oct-1999 to 31-Oct-1999	176.19	13.29	142.90	8.98	85.94	7.11	85.10	3.58
	08-Oct-2013 to 15-Oct-2013	153.94	13.44	97.71	6.95	71.55	8.53	56.01	6.54
	26-Jul-2015 to 05-Aug-2015	150.14	17.36	140.88	8.47	107.38	12.79	117.48	7.94
	09-Oct-2018 to 14-Oct-2018	202.01	12.24	100.85	11.21	83.38	7.54	46.68	7.71
	01-May-2019 to 05-May-2019	210.36	12.35	134.70	15.01	90.67	8.85	40.73	5.75
	07-Aug-1981 to 10-Aug-1981	154.81	13.13	118.06	10.19	74.96	11.16	79.66	8.71
	18-Sep-1985 to 23-Sep-1985	215.82	17.18	64.78	7.51	151.77	15.99	33.71	5.78
	14-Oct-1985 to 18-Oct-1985	181.35	14.71	79.05	6.46	82.34	11.43	44.94	5.24
Mahanadi	07-Nov-1995 to 11-Nov-1995	94.99	6.81	90.11	7.44	62.59	5.77	23.15	3.14
	15-Oct-1999 to 20-Oct-1999	168.80	14.39	68.33	11.45	147.30	11.50	45.24	9.16
	25-Oct-1999 to 31-Oct-1999	179.16	14.49	175.48	9.10	82.00	11.42	127.91	7.79
	08-Oct-2013 to 15-Oct-2013	151.49	10.34	110.79	8.87	108.01	9.26	66.37	7.10
	09-Oct-2018 to 14-Oct-2018	164.62	14.39	167.27	11.46	140.61	14.21	82.51	9.41
	01-May-2019 to 05-May-2019	168.46	13.41	122.79	15.96	146.15	12.12	44.66	8.89
	20-Jul-1989 to 25-Jul-1989	169.52	12.12	68.77	7.98	112.16	10.03	17.84	3.54
	07-Nov-1995 to 11-Nov-1995	162.70	13.52	77.60	8.26	128.96	11.69	24.15	6.46
	13-Nov-1998 to 17-Nov-1998	174.6	14.41	71.59	5.99	126.71	10.42	23.57	3.42
	16-Oct-1999 to 21-Oct-1999	154.49	13.11	91.05	9.14	118.80	11.09	35.34	7.30
Vamshadhabra	13-Dec-2003 to 19-Dec-2003	166.17	13.47	92.77	8.38	92.39	10.09	14.79	3.53
	17-Sep-2005 to 22-Sep-2005	171.48	11.81	142.49	10.31	118.93	9.36	87.81	7.64
	18-May-2010 to 24-May-2010	175.31	9.38	67.39	6.13	117.44	7.22	8.86	1.14
	10-Oct-2013 to 15-Oct-2013	166.17	13.32	149.99	12.98	106.41	9.37	100.23	10.74
	07-Oct-2014 to 16-Oct-2014	175.3	12.23	179.83	17.68	127.33	9.52	85.15	12.62
	09-Oct-2018 to 15-Oct-2018	168.12	12.58	190.87	13.48	129.84	12.09	110.44	10.57

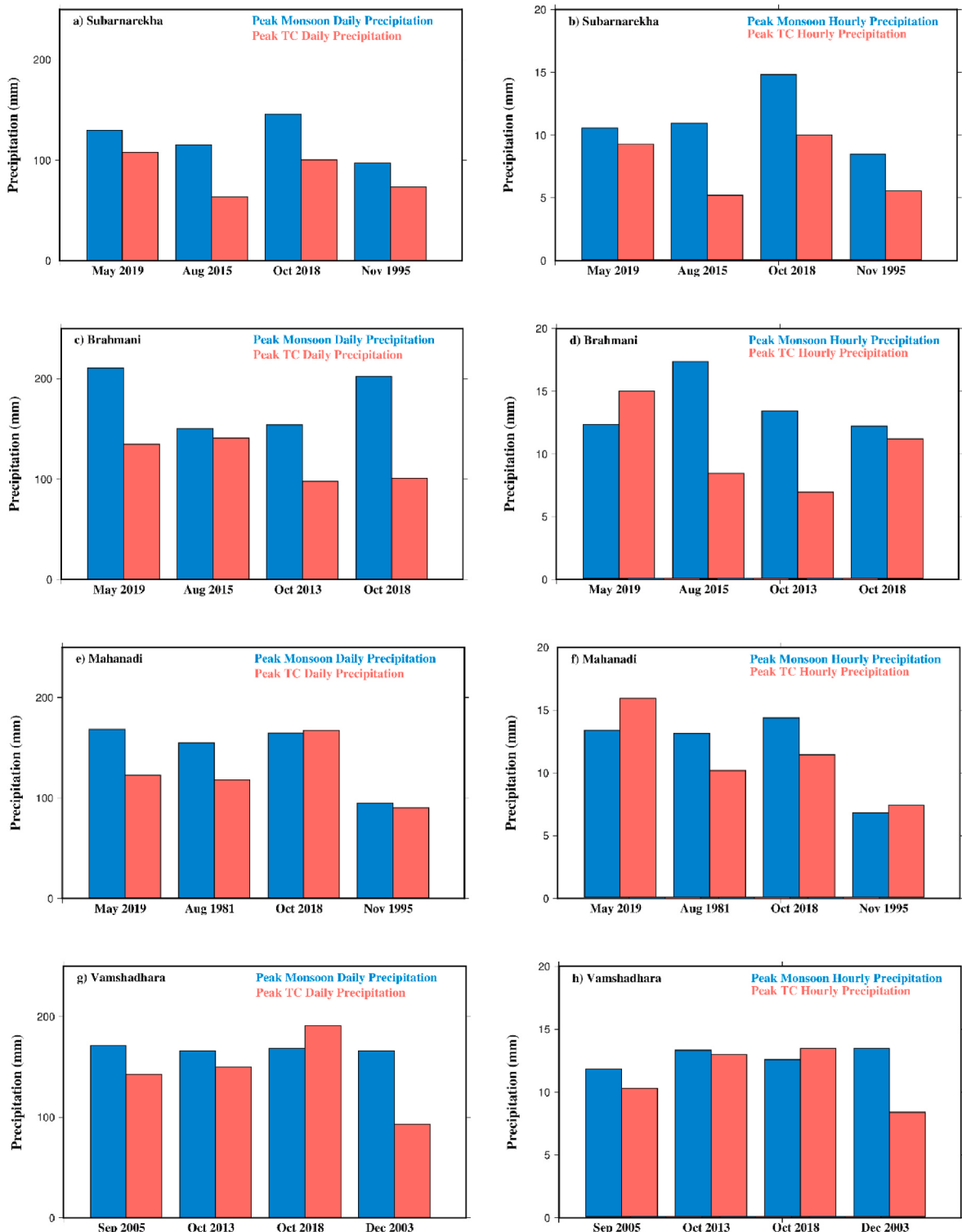


Fig. 4. Comparison of peak daily and hourly precipitation during the summer monsoon period for the TC affected area of various TC events for a-b) Subarnarekha, c-d) Brahmani, e-f) Mahanadi and g-h) Vamshadhara river basins. Here peak monsoon precipitation is taken as the long-term monsoon period peak precipitation (1981–2019).

3.3. Role of precipitation and antecedent soil moisture on TC induced floods

First, we compared precipitation and total runoff during TCs to assess TC-induced rainfall's impact on flooding in the basins. For this, we used the cyclone tracks to estimate the dates during which the cyclones passed over each basin. We identified regions close to the cyclone path

that received heavy precipitation. The daily rainfall and runoff were spatially averaged over the region. We evaluated the peak daily and hourly rainfall and runoff associated with each TC and estimated the long-term peak monsoon rainfall and runoff for each TC affected region (Table 2). A basin wise comparison of peak monsoon daily and hourly rainfall along with the peak TC daily and hourly rainfall for various events for the pre-monsoon, monsoon and post-monsoon seasons was

Table 3

Translation speed and track length of TCs that affected the study area.

Date of TC event	TC Name	Return period of TC induced daily rainfall (Years)	Return period of TC induced hourly rainfall (Years)	TC Translation Speed (km/hr)	Track length (km)	TC Intensity
07-Aug-1981 to 10-Aug-1981	–	11	13	17.04	409	CS
18-Sep-1985 to 23-Sep-1985	–	1	1	22.31	803	CS
14-Oct-1985 to 18-Oct-1985	–	6	2	18.75	1350	SCS
23-May-1989 to 28-May-1989	–	34	19	11.05	1061	SCS
20-Jul-1989 to 25-Jul-1989	–	2	2	24.21	581	CS
07-Nov-1995 to 11-Nov-1995	–	30	39	36.25	1740	VSCS
13-Nov-1998 to 17-Nov-1998	–	2	1	24.64	887	VSCS
15-Oct-1999 to 20-Oct-1999	–	9	7	17.60	1267	VSCS
25-Oct-1999 to 31-Oct-1999	1999 Odisha Cyclone	33	6	13.06	1882	SuCS
13-Dec-2003 to 19-Dec-2003	–	3	2	19.66	1887	SCS
17-Sep-2005 to 22-Sep-2005	Pyarr	18	7	14.65	1055	CS
18-May-2010 to 24-May-2010	Laila	3	2	26.63	1278	SCS
10-Oct-2013 to 15-Oct-2013	Phailin	18	46	15.65	1690	VSCS
07-Oct-2014 to 16-Oct-2014	Hudhud	43	105	13.92	1670	VSCS
26-Jul-2015 to 05-Aug-2015	Komen	21	2	9.53	686	CS
09-Oct-2018 to 15-Oct-2018	Titli	80	30	9.22	885	VSCS
01-May-2019 to 05-May-2019	Fani	20	93	13.51	1946	ESCS

made (Fig. 4). In most cases, the peak TC daily rainfall is comparable with the monsoon peak of that region and the peak TC rainfall does not depend on the season of occurrence. However, the local topography, storm motion, and vertical shear associated with each event strongly influence TC precipitation (Rogers et al., 2009).

We examined the relationship between translation speed and the track length (distance covered before landfall) of each TC and their daily and hourly rainfall return periods (Table 3). Fig. 5 shows the relation between rainfall return periods, translation speed and track length. Here the daily rainfall return periods have moderate negative correlation (-0.48) with the translation speed and a low positive correlation (0.12) with the track length (Fig. 8a and b). The hourly rainfall return periods have a negative correlation (-0.19) with translation speed and a moderate positive correlation (0.50) with the track length (Fig. 8c and d). The higher rainfall return periods are associated with TCs having relatively lower translation speed and longer track length. Moreover, the translation speed has a stronger influence on the daily rainfall accumulation and track length has substantial influence on the hourly rainfall. The TC event of October 1999 (1999 Odisha Cyclone), which caused extremely heavy daily rainfall accumulations with return periods of 34 years and extreme hourly rainfall accumulations with return periods of 6 years, has a relatively low average translation speed of 13 km/h and a track length of approximately 1900 km. However, the November 1998 TC with a relatively meagre daily rainfall return period of 1.5 years had an average translation speed of 24 km/h and a track length of approximately 887 km. In some events, despite the shorter track length, it generates extreme rainfall. For instance, TCs of August 2015 (Komen) and October 2018 (Titli) had relatively short track lengths of 686 and 885 km, respectively, but produced heavy daily rainfall with return periods of 21 and 80 years. The average translation speed of both these TCs was approximately 9 km/h, which is relatively very low. Hence, these TCs having slower translation speeds precipitated over the area for

longer period leading to higher rainfall accumulations. Additionally, the relatively low translation speeds may have aided in extracting more moisture as they moved over the ocean. In the case of TC Komen, the peak hourly rainfall accumulation is comparatively low with a return period of 2 years. Due to the slow movement of the TC, the low hourly rainfall accumulations were distributed over an extended period leading to a high daily rainfall accumulation.

We find a few TCs that caused hourly rainfall with higher return periods compared to the daily rainfall. For instance, the TCs of October 2013 (Phailin), 2014 (Hudhud) and May 2019 (Fani) had extremely high return periods for hourly rainfall compared to that of the daily rainfall. Here, the higher daily rainfall accumulation may be due to the larger size of the TC, as larger TCs can precipitate over a region for longer periods (Titley et al., 2021). The larger size of the TCs maybe related to TC intensities as TCs with higher intensity tend to be larger (Lavender and McBride, 2021). High intensity TCs can also have high hourly rainfall rates in areas close to the centre of the storm, which might have contributed to the heavy hourly rainfall accumulations during these events. The larger size, longer tracks and low translation speed may have caused extreme rainfall during the events. The vertically integrated water vapour flux anomaly over the region during various events were estimated to better understand the influence of larger TCs on rainfall accumulations (Fig. 6). There is a positive anomaly associated with each TC event. In the pre-monsoon and post-monsoon, the positive anomaly in the water vapour flux of TCs is higher, whereas it is lesser for the TCs during the summer monsoon. Subsequently, for TC Phailin and TC Fani, the positive anomaly in the water vapour flux covers a larger area which might have contributed to higher hourly rainfall during these events.

The monsoon peak daily and hourly total runoff was compared with the peak daily and hourly runoff for caused by TCs (Fig. 7). There are several events for which the peak monsoon daily total runoff is comparable with the peak TC daily runoff during the summer monsoon

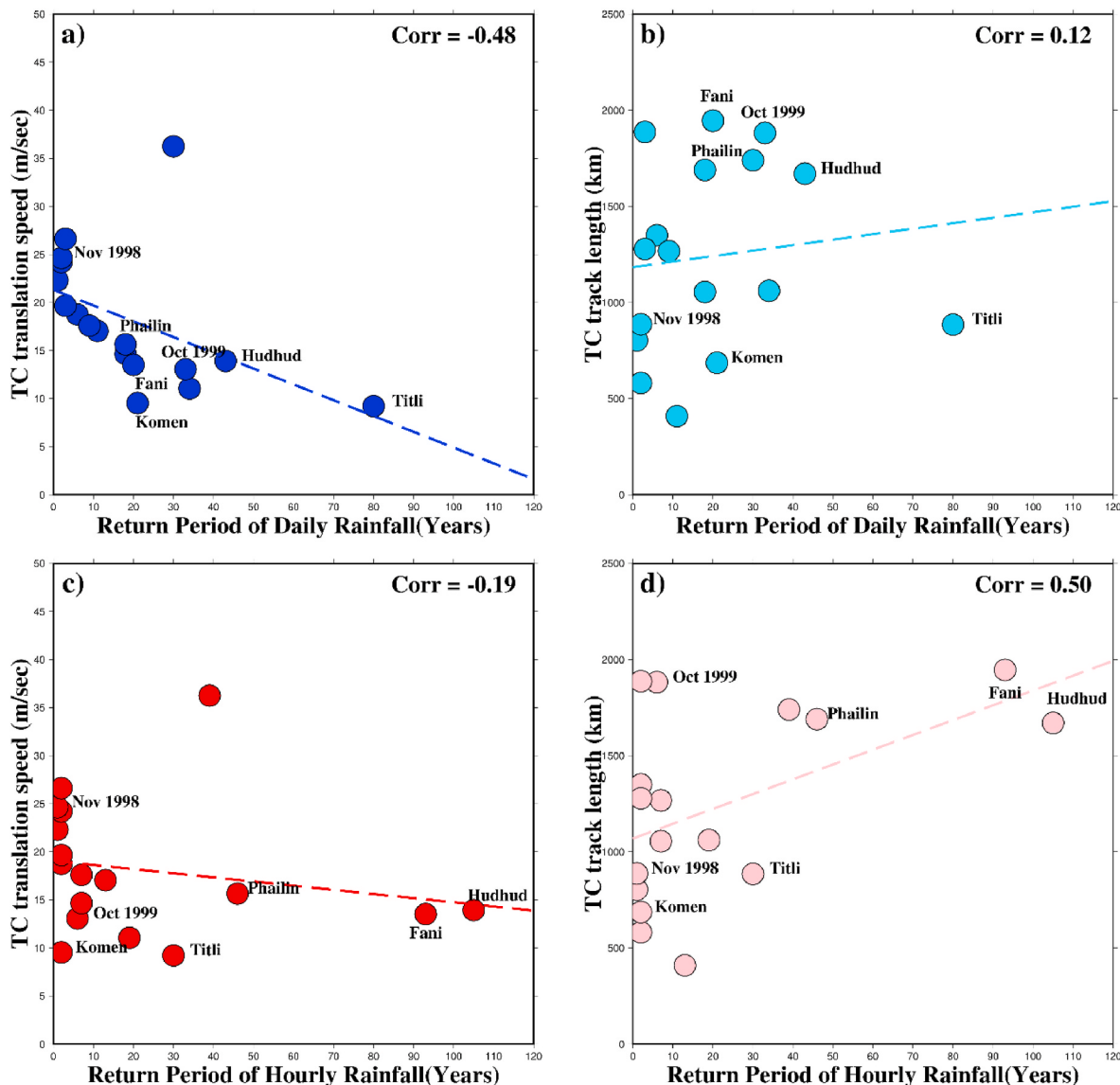


Fig. 5. Relation between daily rainfall return periods and a) translation speed, b) track length and relation between hourly rainfall return periods and c) translation speed, d) track length. The events discussed in section 3.3 are labelled.

season for e.g., the TC event of August 1981, TC Komen and TC Phailin. Moreover, the peak TC hourly runoff generally follows the peak TC hourly rainfall. However, there is a considerable seasonal pattern observed across the basins, particularly in total daily runoff. The pre-monsoon TCs generates relatively low total runoff, and summer monsoon TC events generate relatively high total runoff in each of the four basins. In the post-monsoon during October, just following the monsoon season, TC events generate relatively high runoff whereas, further ahead in the season, the runoff generated by TC is low. This variation in runoff generation shows that flooding due to TCs is not solely dependent on TC rainfall. The return periods of both the peak daily and hourly rainfall and runoff associated with each TC event were estimated (Table 4). Fig. 8 shows the relation between return periods of rainfall and runoff of various TCs. Here, the trend of pre-monsoon events exhibits a steep slope showing that the runoff generated during this period will not be particularly high even when precipitation is high. On the other hand, based on monsoon TCs, the trend shows a gentle slope, suggesting that relatively low precipitation can generate high runoff. Finally, for the post-monsoon period, the trend is moderately sloping with some events exhibiting a behaviour similar to the pre-monsoon events. The spread of the data points shows that the behaviour of

runoff generation during the post-monsoon is more complicated than the other seasons. Hence, we examine in detail the potential of flood generation due to TCs during each season in the next few sections.

3.3.1. Pre-monsoon season

The pre-monsoon period (April–May) is a period of frequent tropical cyclogenesis in the Bay of Bengal. The high intensity of TCs formed during this period may be due to the high ocean heat content, the occurrence of the first branch of the northward propagating intra-seasonal oscillation and its substantial variability (Li et al., 2013). Hence the impact of landfalling TCs during this period is expected to be severe. Here two of the most severe TC events that affected the region during the pre-monsoon are used. The TC event of May 1989 and TC Fani have impacted multiple basins in the area. The TC event in May 1989 has caused extreme mean daily rainfall accumulation over the region with a return period of 34 years and hourly rainfall accumulation with a return period of 19 years in the Subarnarekha basin, which is considerably higher than the rainfall from other TC events in the basin. However, the daily runoff generated in that region due to the TC event is relatively low, having a return period of approximately 9 years. Previous studies also show that the event resulted in flooding along the coasts with no

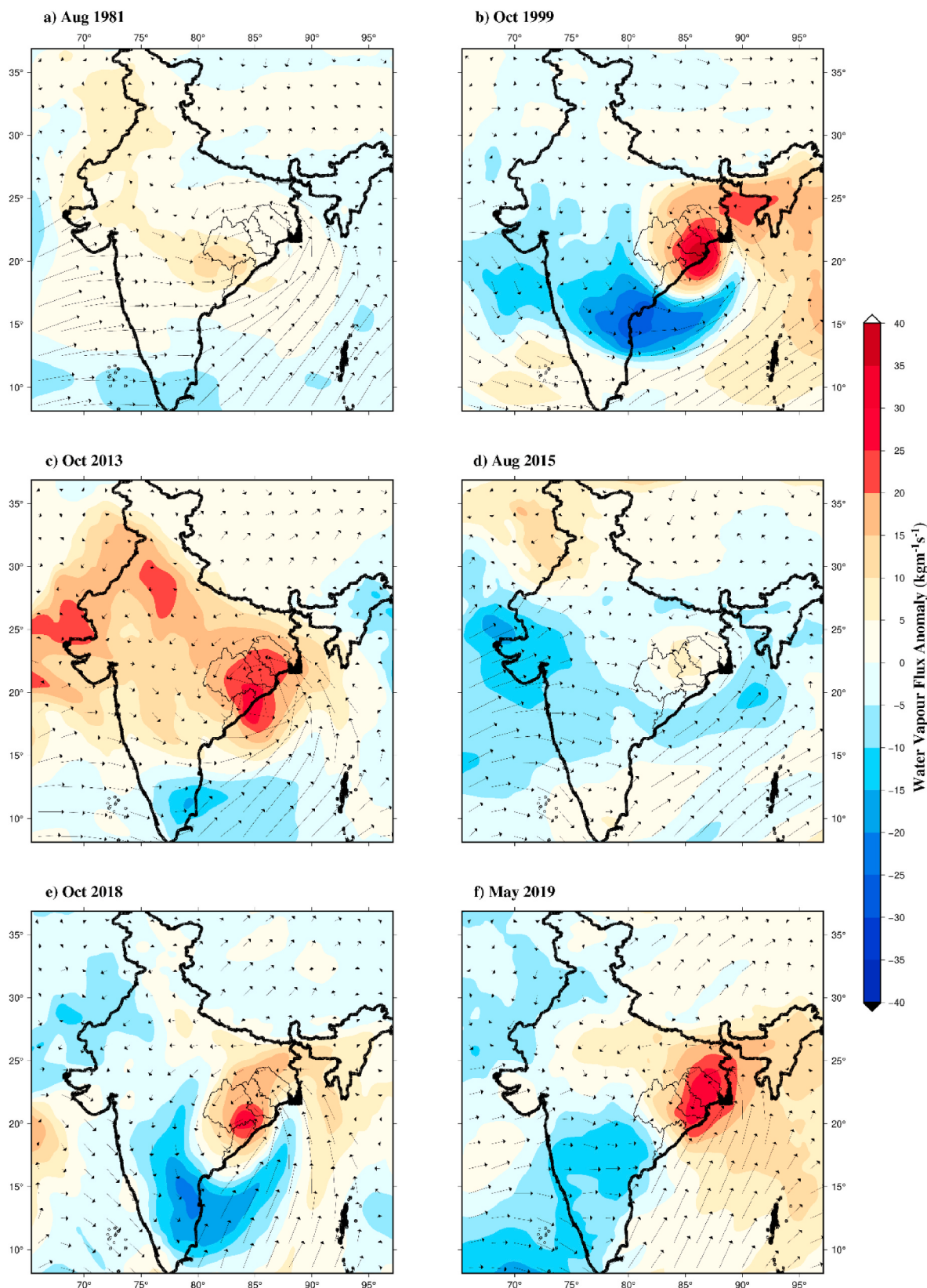


Fig. 6. Vertically integrated water vapour flux anomaly ($\text{kg m}^{-1} \text{s}^{-1}$) associated with TCs that occurred in a) August 1981, b) October 1999, c) October 2013, d) August 2015, e) October 2018, and f) May 2019. The vectors here represent the wind speed at 850 hPa in the region.

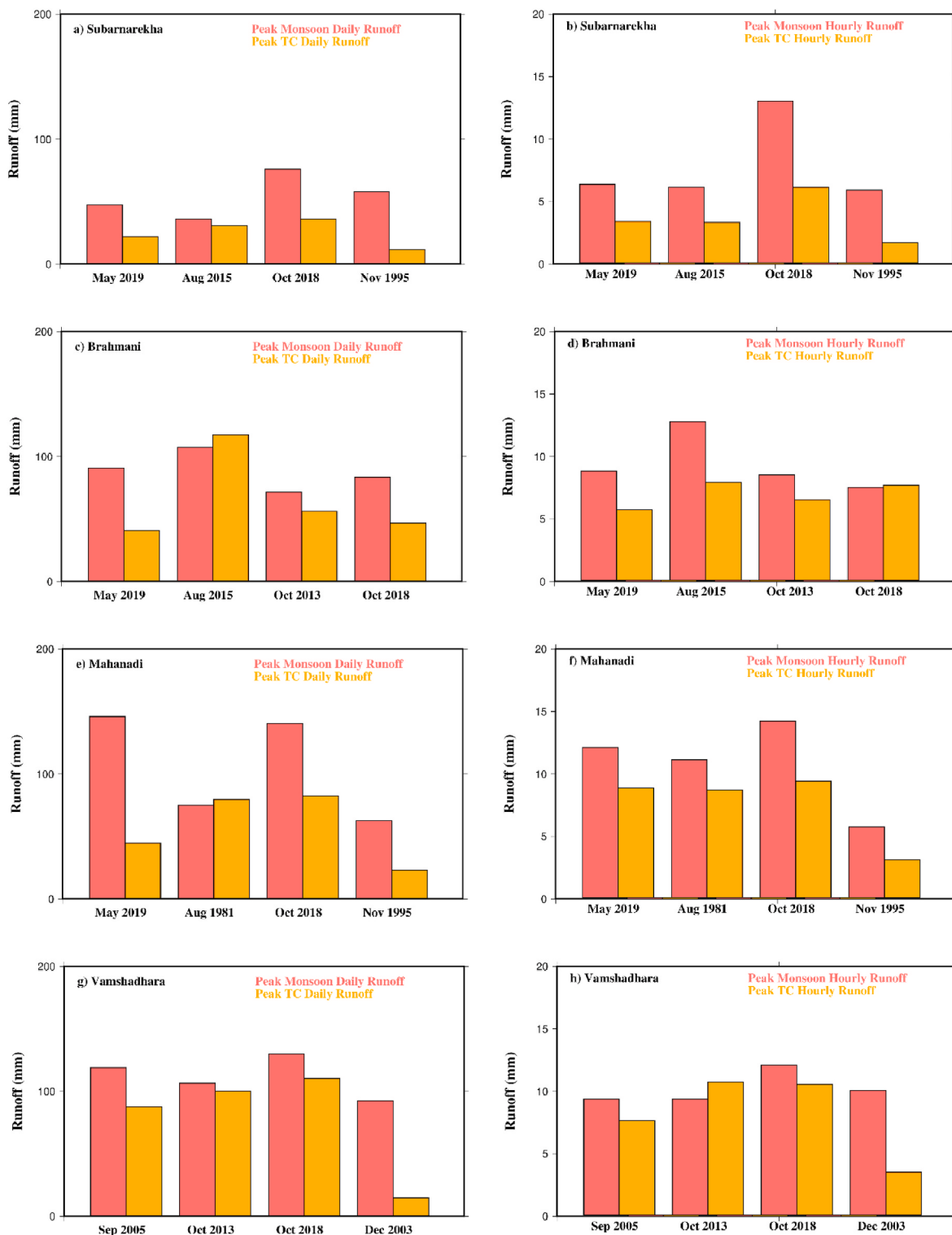


Fig. 7. Comparison of peak daily and hourly total runoff during the summer monsoon period for the TC affected area of various TC events for a-b) Subarnarekha, c-d) Brahmani, e-f) Mahanadi and g-h) Vamshadvara river basins. Here peak monsoon runoff is taken as the long-term monsoon period peak runoff (1981–2019).

substantial flooding in the basin's interior (Chittibabu et al., 2004). The flooding along the coast may be due to the storm surge associated with the TC, which reached up to 6 m in certain parts of the region.

In the case of TC Fani, extreme daily rainfall with return periods of 12, 20, and 8 years occurred in the Subarnarekha, Brahmani, and Mahanadi basins. However, the estimated return periods of daily and hourly runoff generated in each basin was less than five years. Previous

studies reported that most of the damage was due to the extreme wind despite flooding in the coastal and low-lying areas, primarily due to storm surge (RSMC, 2020). The reduced runoff generation in the basin's interior during this period can be due to the reduced soil moisture content of the basins during the pre-monsoon season. The 7-day soil moisture percentile for the area before TC Fani shows that the soil moisture percentile across the basins is less than 40% (Fig. 9a). The

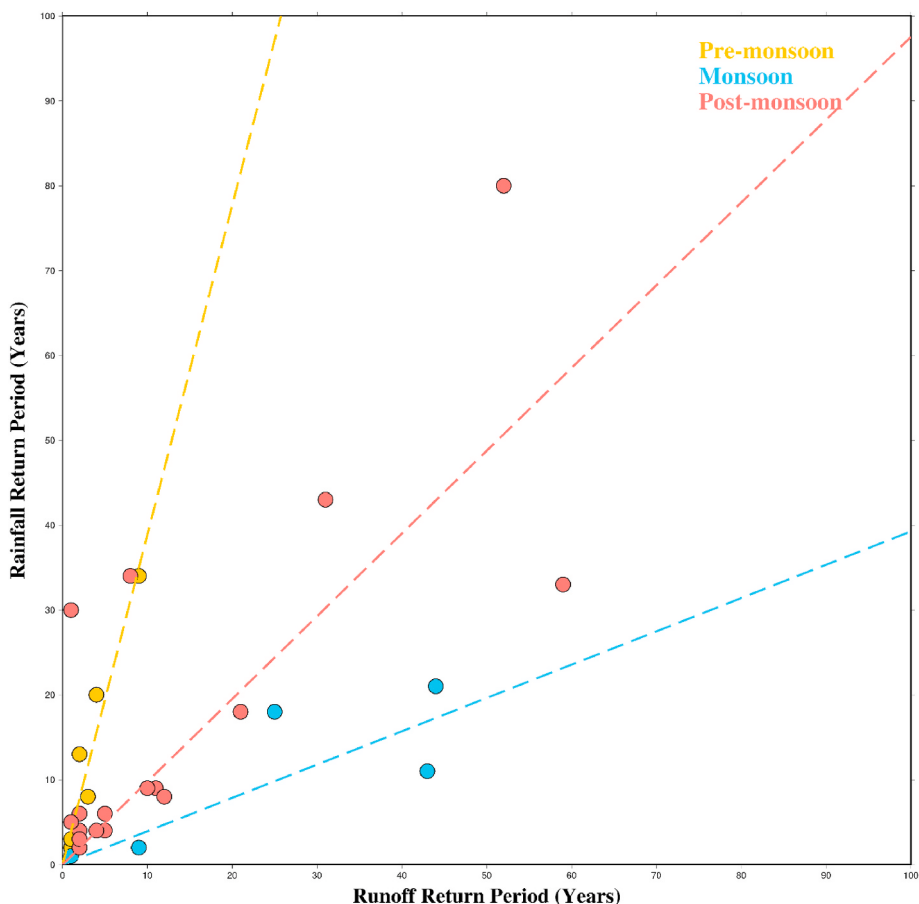


Fig. 8. Relation between daily rainfall return periods and daily runoff return periods. Yellow corresponds to pre-monsoon TCs, blue to monsoon TCs and red to post-monsoon TCs. Trend lines of each season is also plotted. (For interpretation of the references to colour in this figure legend, the reader is referred to the Web version of this article.)

precipitation, total runoff, and soil moisture content during this period over the Brahmani basin was compared (Fig. 10a). We find that the TC generated severe rainfall accumulation (>120 mm/day) over the region. However, the runoff peak associated with the event is particularly low. The soil moisture percentiles before the TC event show very low soil moisture levels (less than 20th percentile). A large fraction of the rainfall contributed primarily to elevating soil water content in the basin. Hence, any rainfall caused by TCs during the pre-monsoon (e.g. TC Fani, TC Laila, May 1989 TC) may not cause serious flooding due to drier antecedent moisture conditions.

3.3.2. Summer monsoon

The frequency of TC formation is considerably less during the summer monsoon (June–September). However, TCs do occur but will usually be of lower intensities than those in the pre-monsoon and post-monsoon. Strong vertical shear, decreased absolute vorticity, and lower maximum potential intensity contributes to reducing the frequency of TCs in the monsoon period, all of which work to overcome the increased relative humidity effect that favours TC formation (Li et al., 2013). We consider five different TCs, namely August 1981 TC, September 1985 TC, July 1989 TC, Pyarr (2005) and Komen (2015) that affected the area during the monsoon period of 1981–2019, to assess the TC induced flooding. In most cases, the daily TC rainfall generates daily runoff having high return periods, which suggests the occurrence of severe floods during such events. However, the return period of hourly TC rainfall is low, affecting the hourly runoff return periods. An example of such an event is TC Komen that caused flooding and landslides resulting in severe damage to human lives and infrastructure in Odisha and West Bengal (RSMC, 2016). Wetter antecedent soil moisture during

the summer monsoon contributes to flooding as rainfall can directly contribute to overland flow. We find wetter soil moisture in all the four basins before the TC in July 2015, with most of the region having a 7-day soil moisture percentile higher than 80th percentile (Fig. 9b). Comparison of daily precipitation, total runoff, and soil moisture for this event over the Brahmani basin shows that extreme precipitation (140 mm) and wet soil moisture (~80th percentile) in the region resulted in extreme runoff (117 mm) (Fig. 10b). In the Mahanadi basin, the TC of August 1981 resulted in flooding that affected a large part of the basin (Chittibabu et al., 2004). Higher daily runoff generated during this event was associated with wet soil moisture. We also note the effect of elevated soil moisture during monsoon in the Vamshadhara basin during the September 2005 TC (Pyarr) [Fig. 12a], which resulted in heavy flooding (RSMC, 2006). Hence, even though TCs have low frequency and intensity during the monsoon period, any TC that does make landfall is likely to produce severe floods in the region as the antecedent moisture condition is high in each basin.

3.3.3. Post-monsoon season

The post-monsoon (October–November) is a period with high TC frequency. However, compared to the pre-monsoon period, the intensity of TCs formed during this period is less (Li et al., 2013; Neetu et al., 2019). The higher frequency of cyclogenesis in the Bay of Bengal during this period can lead to temporally compounding TCs, leading to flooding (Zscheischler et al., 2020). Following the summer monsoon, soil moisture in the basins starts to decrease over time. Therefore, despite the heavy rainfall associated with many TCs, they fail to cause severe floods in the basins during this period. The effect of drier antecedent soil moisture of the basins can be observed in the TC of November 1995. The

Table 4

Return period of rainfall and total runoff associated with TCs.

Basin	Date of TC event	Return period of TC induced daily rainfall (Years)	Return period of TC induced hourly rainfall (Years)	Return period of daily runoff (Years)	Return period of total runoff (Years)
Subarnarekha	14-Oct-1985 to 18-Oct-1985	6	2	2	2
	23-May-1989 to 28-May-1989	34	19	9	11
	07-Nov-1995 to 11-Nov-1995	5	3	1	1
	15-Oct-1999 to 20-Oct-1999	9	7	11	10
	25-Oct-1999 to 31-Oct-1999	2	2	2	2
	31-Jul-2015 to 06-Aug-2015	2	2	9	3
	10-Oct-2018 to 16-Oct-2018	6	9	5	6
	01-May-2019 to 05-May-2019	13	11	2	2
	07-Nov-2019 to 12-Nov-2019	2	1	2	1
Brahmani	14-Oct-1985 to 18-Oct-1985	4	2	5	2
	23-May-1989 to 28-May-1989	2	2	1	1
	15-Oct-1999 to 20-Oct-1999	4	7	2	2

Table 4 (continued)

Basin	Date of TC event	Return period of TC induced daily rainfall (Years)	Return period of TC induced hourly rainfall (Years)	Return period of daily total runoff (Years)	Return period of hourly total runoff (Years)
	Oct-1999				
	25-Oct-1999 to 31-Oct-1999	33	6	59	5
	08-Oct-2013 to 15-Oct-2013	8	2	12	4
	26-Jul-2015 to 05-Aug-2015	21	2	44	4
	09-Oct-2018 to 14-Oct-2018	9	29	10	36
Mahanadi	01-May-2019 to 05-May-2019	20	93	4	3
	07-Aug-1981 to 10-Aug-1981	11	13	43	19
	18-Sep-1985 to 23-Sep-1985	1	1	1	2
	14-Oct-1985 to 18-Oct-1985	2	1	2	2
	07-Nov-1995 to 11-Nov-1995	30	39	1	2
	15-Oct-1999 to 20-Oct-1999	2	8	2	6
	25-Oct-1999 to 31-Oct-1999	47	3	183	4
	08-Oct-2013 to 15-Oct-2013	4	10	4	7

(continued on next page)

Table 4 (continued)

Basin	Date of TC event	Return period of TC induced daily rainfall (Years)	Return period of TC induced hourly rainfall (Years)	Return period of daily total runoff (Years)	Return period of hourly total runoff (Years)
	Oct-2013				
	09-	34	10	8	6
	Oct-2018				
	to 14-				
	Oct-2018				
	01-May-2019	8	94	3	4
	to 05-May-2019				
Vamshadharा	20-Jul-1989	2	2	2	2
	to 25-Jul-1989				
	07-Nov-1995	2	2	2	2
	to 11-Nov-1995				
	13-Nov-1998	2	1	2	1
	to 17-Nov-1998				
	16-Oct-1999	2	2	2	3
	to 21-Oct-1999				
	13-Dec-2003	3	2	2	2
	to 19-Dec-2003				
	17-Sep-2005	18	7	25	11
	to 22-Sep-2005				
	18-May-2010	3	2	1	1
	to 24-May-2010				
	10-Oct-2013	18	46	21	68
	to 15-Oct-2013				
	07-Oct-2014	43	105	31	55
	to 16-Oct-2014				
	09-Oct-2018	80	30	52	16
	to 15-				

Table 4 (continued)

Basin	Date of TC event	Return period of TC induced daily rainfall (Years)	Return period of TC induced hourly rainfall (Years)	Return period of daily total runoff (Years)	Return period of hourly total runoff (Years)
	Oct-2018				

7-day soil moisture percentile before the TC is less than 80% for most basins (Fig. 9d). Before the TC event in the Mahanadi basin, soil moisture content is approximately 60% and did not produce substantial runoff even though the rainfall associated with the event was substantial (Fig. 11d).

Prior to the TC Titli, the 7-day soil moisture percentile over most basins was less than 80% (Fig. 9c). In the Mahanadi basin, we note a TC rainfall driven increase in soil moisture from less than 70th to 100th percentile during 10–12 October 2018. This increase in soil moisture suggests that a fraction of TC rainfall had constantly contributed to increase the soil water content reducing runoff generation (Fig. 11c). Hence, the return period of runoff (3.87 years) associated with this event shows that only minor flooding occurred despite severe rainfall in the basin. However, in the Vamshadharā basin, severe flooding did occur due to the TC Titli (RSMC, 2019). The comparison of rainfall, runoff, and soil moisture for this event over the Vamshadharā basin shows that the daily precipitation was distributed over two days with the second day receiving heavy rainfall (Fig. 12d). Moreover, compared to the Mahanadi basin where rainfall exhibited a similar temporal distribution, the Vamshadharā basin received higher rainfall on the first day causing a rapid elevation of soil moisture in the basin leading faster saturation. Due to rapid saturation and heavy rainfall (80-year return period) on October 11, 2018, the rate of infiltration of water over the region had reduced and the fraction of rainfall contributing to total runoff had increased.

There are also other TCs during the post-monsoon that caused floods. For example, the 1999 Odisha Cyclone, TC Phailin, and TC Hudhud have led to severe flooding (Parida et al., 2018; RSMC, 2014, 2000). The impact of TC Phailin on Brahmani and Vamshadharā basin exhibits elevated antecedent soil moisture (>80th percentile) before the TC event (Figs. 10d and 12b). In the Brahmani basin, these high soil moisture conditions aided in generating severe daily runoff (with return periods of 12 years) even though the daily rainfall accumulation over the region was considerably low (with a return period of 8 years). However, in the Vamshadharā basin, elevated soil moisture and the heavy TC daily rainfall accumulations (return period of 18 years) led to severe flooding (return period of 21 years) in the basin. This increase in soil moisture could be because of the reduction in time between monsoon withdrawal and TC formation, which aid in maintaining high antecedent soil moisture in the basins.

The 1999 Odisha cyclone caused extreme flooding even though it occurred towards the end of October when the antecedent soil moisture conditions are usually low. Here two TCs consecutively made landfall in the exact location. The first of them occurred during mid-October and affected all four basins but did not cause extensive flooding as antecedent soil moisture had started to decrease after the summer monsoon season. However, published reports show that the second TC affected the coastal region of Subarnarekha, Brahmani, and Mahanadi basins leading to extreme flooding in the two basins (RSMC, 2000). In addition to the severe rainfall associated with them, the increase in antecedent soil moisture following the first TC event may have influenced runoff generation during the second TC event causing extreme flooding in the basins. It is also worth noting that the severity of the second TC was stronger than the first one which may also have influenced flooding. The influence of TC rainfall of October 1999 on the region's runoff and soil moisture is shown in Figs. 10c and 11b. Hence, the likelihood of flooding

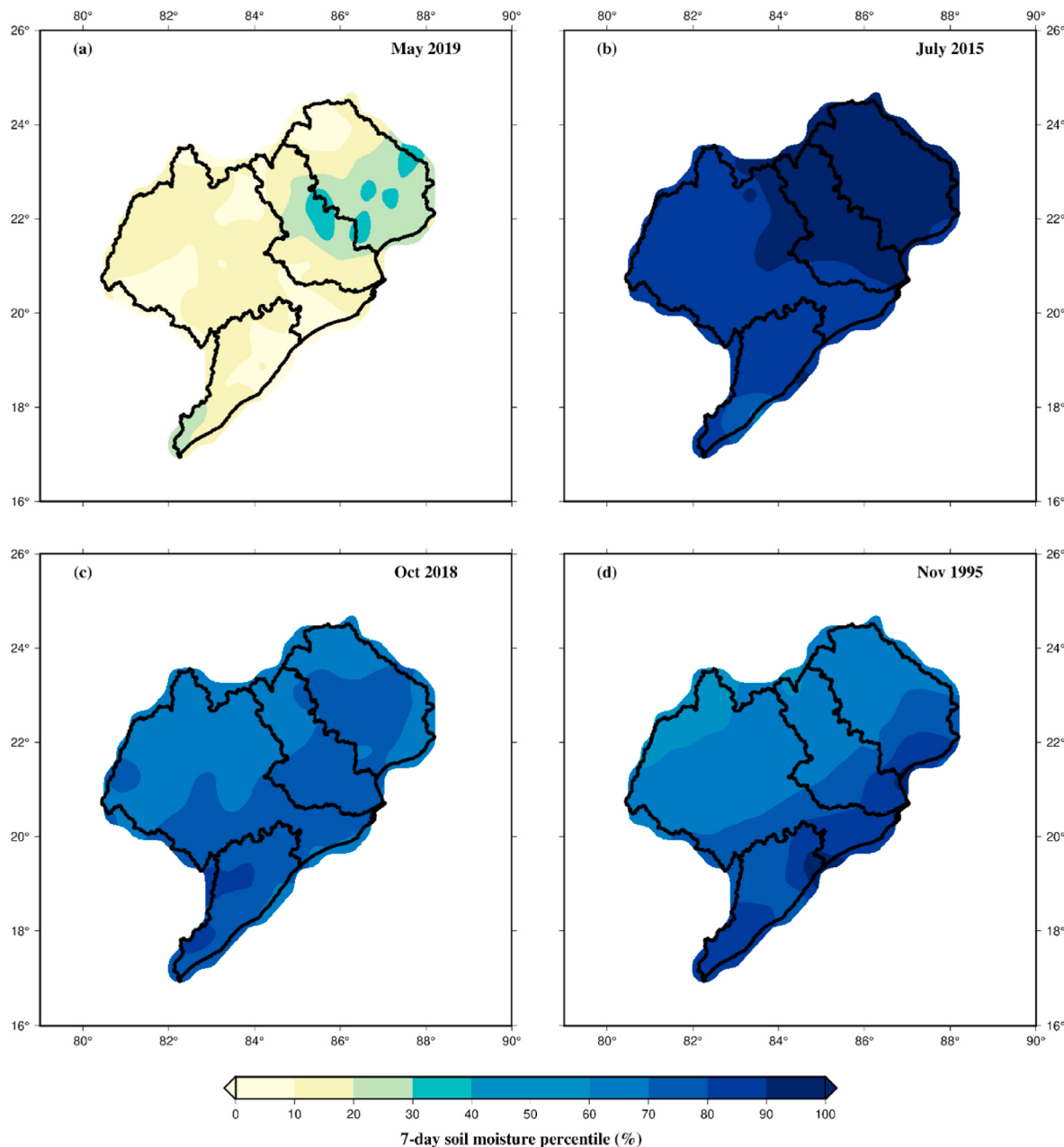


Fig. 9. Spatial distribution of 7-day soil moisture percentiles prior to TC events in a) May 2019, b) July 2015, c) October 2018, and d) November 1995.

is high during the early post-monsoon period following the summer monsoon, which gradually decreases with time.

4. Discussion and conclusion

Understanding the influence of TCs on flooding is vital to minimize the damage due to landfalling TCs. Previous studies have explored the potential of TCs to cause flooding overland (Gori et al., 2020; Macaladal et al., 2021; Titley et al., 2021; Villarini et al., 2014). For instance, Gori et al. (2020) used a simplified physical model to derive the primary drivers leading to compound flooding due to TCs in the Cape Fear River, USA. Furthermore, Villarini et al. (2014) investigated the role of large-scale climate indices in TC induced flooding over the continental USA. Previous efforts to assess the vulnerability towards TC induced floods in India have primarily focused on the coastal region (Dube et al., 2009; Rao et al., 2007, 2015; Sahoo and Bhaskaran, 2018). However, studies have shown that TCs can lead to extensive flooding further

inland (Bahinipati, 2014; Titley et al., 2021; Villarini et al., 2014). We assess the impact of TCs on flooding in four major Indian river basins from 1981 to 2019. A primary driver of TC-induced flooding is the heavy rainfall associated with TCs. Consistent with previous studies (Rogers et al., 2009; Titley et al., 2021), we find that the TC rainfall accumulations depends on the size of TCs, translation speed, and the distance travelled before making landfall. Kossin (2018) reported a reduction in the translation rate of TCs weakening of the summertime tropical circulations due to climate change, which can further affect the severity of TC induced flooding. Additionally, we find a seasonal influence in runoff generation due to TCs having similar mean daily rainfall accumulations. This seasonal variation in TC induced flooding suggests that other drivers also play a role in TC-induced flooding in addition to rainfall.

Previous studies (Berghuijs et al., 2019; Titley et al., 2021; Garg and Mishra, 2019; Sharma et al., 2018) demonstrated the significance of antecedent soil moisture in flooding. In the pre-monsoon period, during which the antecedent soil moisture in the basins is low, severe TC

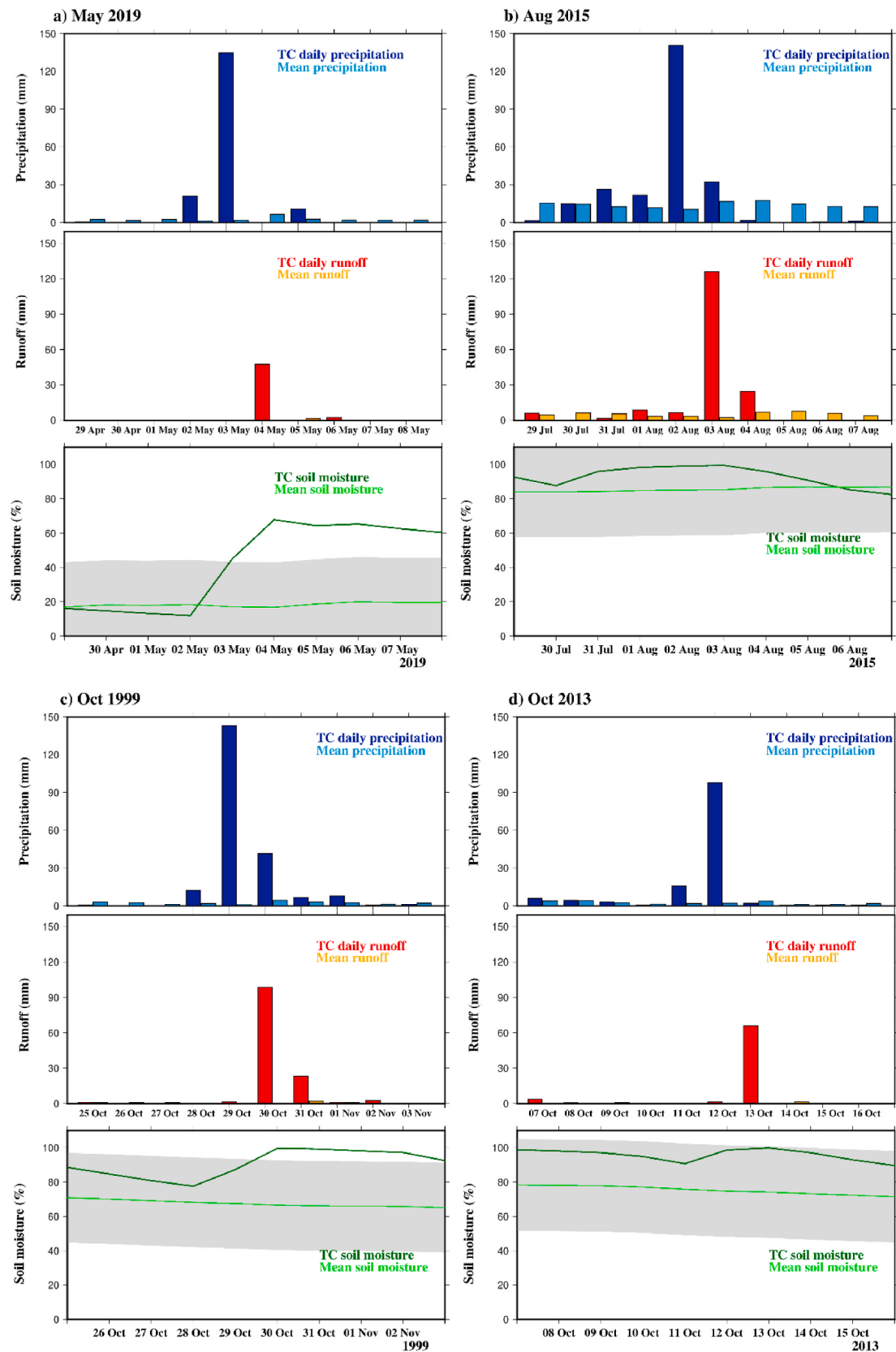


Fig. 10. Comparison of daily precipitation, total runoff, and soil moisture percentile associated with TCs of a) May 2019, b) August 2015, c) October 1999, and d) October 2013 in Brahmani basin. The long term mean daily precipitation, runoff and soil moisture percentile (± 1 standard deviation) for this period are also provided.

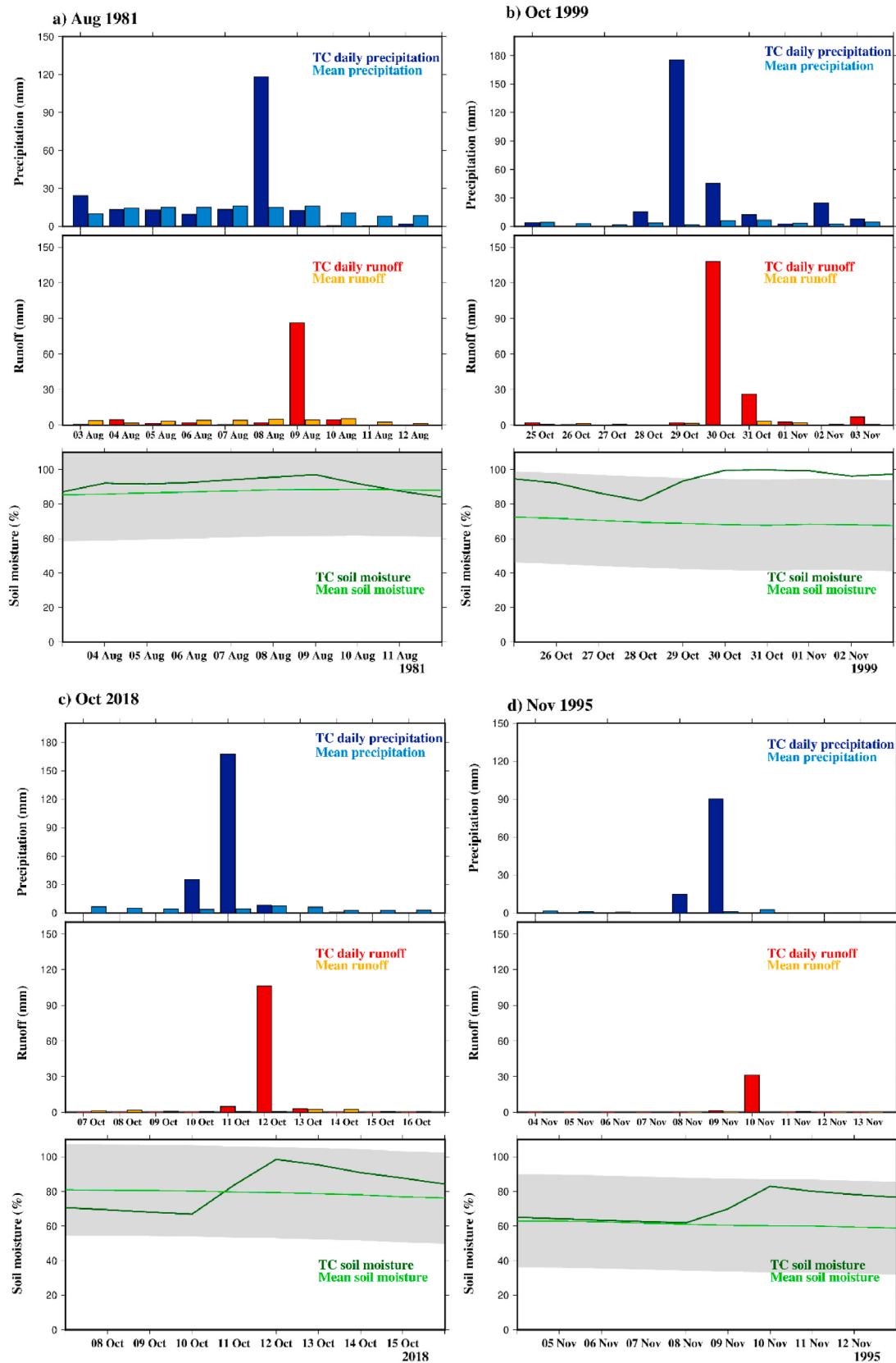


Fig. 11. Comparison of daily precipitation, runoff and soil moisture percentile associated with TC events of a) August 1981, b) October 1999, c) October 2018, and d) November 1995 in Mahanadi basin. The long term mean daily precipitation, runoff and soil moisture percentile (± 1 standard deviation) for this period are also provided.

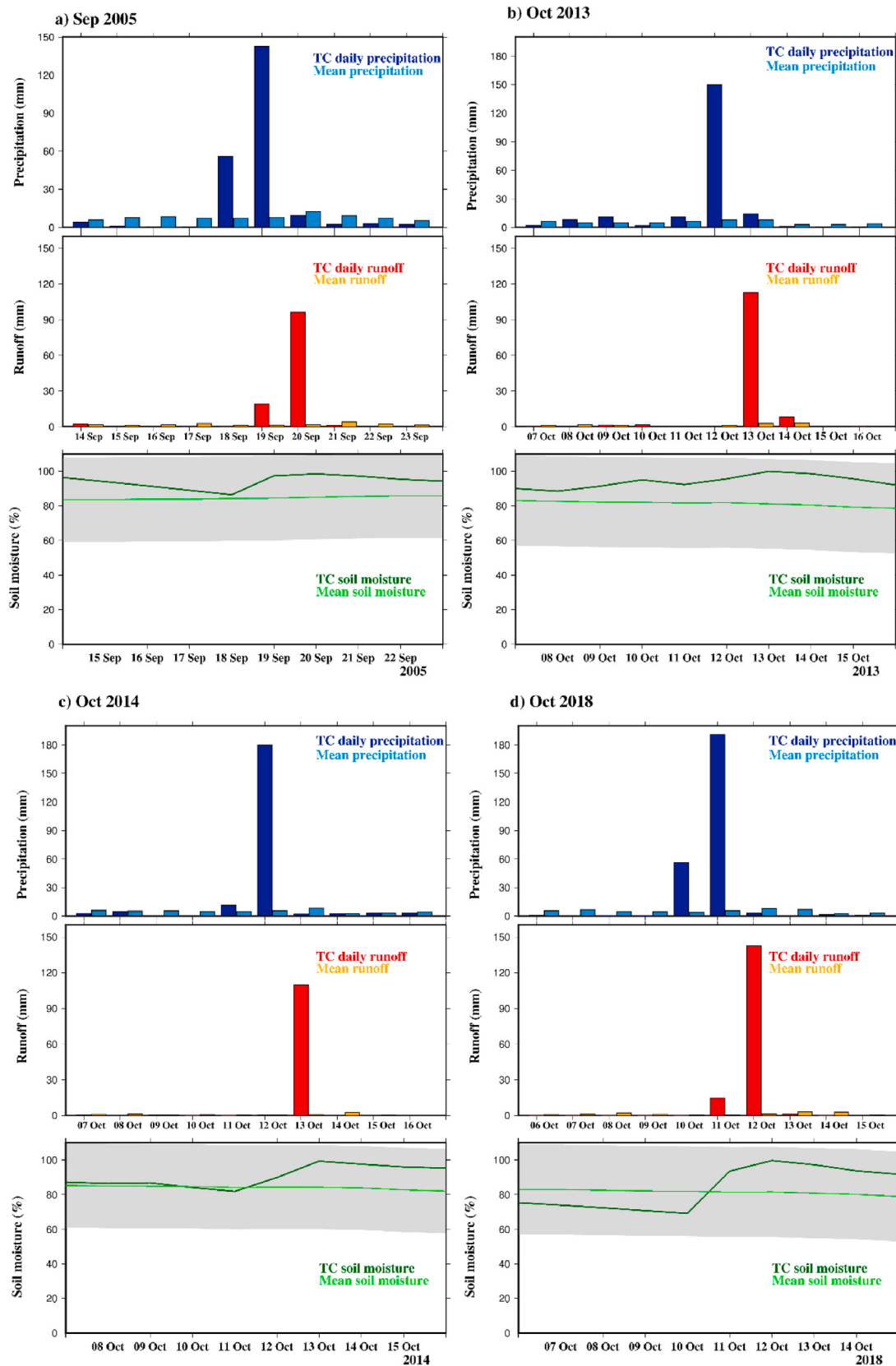


Fig. 12. Comparison of daily precipitation, runoff and soil moisture percentile associated with TC events a) September 2005, b) October 1999, c) October 2014, and d) October 2018 in Vamshadhara basin. The long term mean daily precipitation, runoff and soil moisture percentile (± 1 standard deviation) for this period are also provided.

induced flooding does not occur despite considerable rainfall. Hence, despite TCs with high mean daily rainfall accumulations during this period, the potential of severe flooding remains low. This can be observed for TC Fani, which caused heavy rainfall in Brahmani, Mahanadi, and Subarnarekha basins but did not cause flooding (RSMC, 2020). However, even though cyclogenesis is low during the summer monsoon period, the river basins are saturated. Therefore, any TC that makes landfall during this period has a high potential to cause severe flooding. For example, reports show that TC Pyarr caused heavy flooding in the Vamshadbara basin even though the TC was classified as a Cyclonic Storm (CS) (RSMC, 2006). In the post-monsoon period, TC induced flooding primarily depends on the period of occurrence of TC. This is because, following the summer monsoon, the antecedent soil moisture starts to decrease with time. Hence, TC events at the beginning of this period can cause floods. TC Phailin, which caused flooding in the Brahmani, Mahanadi and Vamshadbara basins (RSMC, 2014), is an example of TC event that caused flooding in this period. On the other hand, the TC of November 1995 that affected the Mahanadi basin (Annual RSMC Report, 1996) demonstrates the lack of TC induced flooding further into the post-monsoon despite heavy rainfall. However, the increased frequency of TCs during this period may lead to temporal clustering of TCs (Paliwal and Patwardhan, 2013; Zscheischler et al., 2020). The impact of clustering TCs on flooding can be observed during the cyclone season of October 1999, when two TCs affected both the Brahmani and Mahanadi basins within a short period (RSMC, 2000).

Based on our findings, the major conclusions are:

1. In the Indian region, landfalling TCs do have the potential to cause floods in the river basins. Both TC rainfall and antecedent soil moisture of the basin controls the severity of floods.
2. The landfalling TCs caused heavy mean daily rainfall accumulations over the regions with maximum return periods of 34, 33, 46 and 80 years in Subarnarekha, Brahmani, Mahanadi and Vamshadbara basin, respectively. TC rainfall depends on the translation speed and size of TCs, with slower and larger TCs causing higher rainfall accumulations.
3. Landfalling TCs in the pre-monsoon season is less likely to cause severe flooding. The antecedent soil moisture in the basins will be very low during this period, and the rainfall from the TCs contributes primarily to the soil water content of the basin. During this period, the return period of daily runoff has relatively low return periods of 9, 4, 3 and 2 years in Subarnarekha, Brahmani, Mahanadi and Vamshadbara basin, respectively.
4. TCs can cause severe flooding during the monsoon period with return periods of 9, 44, 43 and 25 years in Subarnarekha, Brahmani, Mahanadi, and Vamshadbara basin. In this period, the high soil moisture conditions of the basin cause the TC rainfall to be directly converted into runoff. The severity of flooding during this period primarily depends on the rainfall associated with the TC.
5. In the post-monsoon period, the potential of flooding primarily depends on the antecedent soil moisture of the basin. When antecedent soil moisture is high, the likelihood of TC-induced flooding increases, particularly following the monsoon period or due to the clustering of TCs. Hence, in addition to TC track prediction, to minimize damage from TCs, it is crucial to monitor the basin characteristics.

Author statement

Vimal Mishra: Conceptualization, analysis, writing; Akshay Rajeev: Analysis, writing.

Declaration of competing interest

The authors declare that they have no known competing financial interests or personal relationships that could have appeared to influence the work reported in this paper.

Acknowledgements

Authors acknowledge the financial assistance from the Ministry of Education and Ministry of Earth Sciences. Data availability from the India Meteorological Department (IMD) and ERA-5 is greatly appreciated.

Appendix A. Supplementary data

Supplementary data to this article can be found online at <https://doi.org/10.1016/j.wace.2022.100432>.

References

- Annual RSMC Report, 1996. REPORT on CYCLONIC DISTURBANCES over NORTH INDIAN OCEAN during 1995, Annual RSMC Report. INDIA METEOROLOGICAL DEPARTMENT, New Delhi.
- Bahinipati, C.S., 2014. Assessment of vulnerability to cyclones and floods in Odisha, India: a district-level analysis. *Curr. Sci.* 107, 1997–2007.
- Balaguru, K., Taraphdar, S., Leung, L.R., Foltz, G.R., 2014. Increase in the intensity of postmonsoon Bay of Bengal tropical cyclones. *Geophys. Res. Lett.* 41, 3594–3601. <https://doi.org/10.1002/2014GL060197>.
- Berghuijs, W.R., Harrigan, S., Molnar, P., Slater, L.J., Kirchner, J.W., 2019. The relative importance of different flood-generating mechanisms across europe. *Water Resour. Res.* 55, 4582–4593. <https://doi.org/10.1029/2019WR024841>.
- Bhardwaj, P., Pattanaik, D.R., Singh, O., 2019. Tropical cyclone activity over Bay of bengal in relation to El niño-southern oscillation. *Int. J. Climatol.* 39, 5452–5469. <https://doi.org/10.1002/joc.6165>.
- Brunke, M.A., Cassano, J.J., Dawson, N., DuVivier, A.K., Gutowski Jr., W.J., Hamman, J., Maslowski, W., Nijssen, B., Reeves Eyre, J.E.J., Renteria, J.C., Roberts, A., Zeng, X., 2018. Evaluation of the atmosphere–land–ocean–sea ice interface processes in the Regional Arctic System Model version 1 (RASM1) using local and globally gridded observations. *Geosci. Model Dev. (GMD)* 11, 4817–4841. <https://doi.org/10.5194/gmd-11-4817-2018>.
- Chen, Y., Sharma, S., Zhou, X., Yang, K., Li, X., Niu, X., Hu, X., Khadka, N., 2021. Spatial performance of multiple reanalysis precipitation datasets on the southern slope of central Himalaya. *Atmos. Res.* 250, 105365. <https://doi.org/10.1016/j.atmosres.2020.105365>.
- Chittibabu, P., Dube, S.K., Macnabb, J.B., Murty, T.S., Rao, A.D., Mohanty, U.C., Sinha, P.C., 2004. Mitigation of flooding and cyclone hazard in Orissa, India. *Nat. Hazards* 31, 455–485. <https://doi.org/10.1023/B:NHAZ.0000023362.26409.22>.
- Cyclone eAtlas-IMD, 2021. WEB Cyclone ATLAS::AboutEAtlas [WWW Document]. URL. <http://14.139.191.203/AboutEAtlas.aspx>.
- Dube, S.K., Jain, I., Rao, A.D., Murty, T.S., 2009. Storm surge modelling for the Bay of bengal and arabian sea. *Nat. Hazards* 51, 3–27. <https://doi.org/10.1007/s11069-009-9397-9>.
- Evan, A.T., Camargo, S.J., 2011. A climatology of arabian sea cyclonic storms. *J. Clim.* 24, 140–158. <https://doi.org/10.1175/2010JCLI3611.1>.
- Girishkumar, M.S., Ravichandran, M., 2012. The influences of ENSO on tropical cyclone activity in the Bay of Bengal during October–December: ENSO influence ON bay cyclone. *J. Geophys. Res.* 117 <https://doi.org/10.1029/2011JC007417> n/a-n/a.
- Gori, A., Lin, N., Xi, D., 2020. Tropical cyclone compound flood hazard assessment: from investigating drivers to quantifying extreme water levels. *Earth's Future* 8, e2020EF001660. <https://doi.org/10.1029/2020EF001660>.
- Gray, W.M., 1968. Global view OF the origin OF tropical disturbances and storms. *Mon. Weather Rev.* 32.
- Hamlet, A.F., Elsner, M.M., Mauger, G.S., Lee, S.-Y., Tohver, I., Norheim, R.A., 2013. An overview of the columbia basin climate change scenarios project: approach, methods, and summary of key results. *Atmos.-Ocean* 51, 392–415. <https://doi.org/10.1080/07055900.2013.819555>.
- Hamman, J., Nijssen, B., Roberts, A., Craig, A., Maslowski, W., Osinski, R., 2017. The coastal streamflow flux in the regional arctic System model. *J. Geophys. Res.: Oceans* 122, 1683–1701. <https://doi.org/10.1002/2016JC012323>.
- Hoarau, K., Bernard, J., Chalonge, L., 2012. Intense tropical cyclone activities in the northern Indian Ocean: intense tropical cyclones activity IN the northern INDIAN ocean. *Int. J. Climatol.* 32, 1935–1945. <https://doi.org/10.1002/joc.2406>.
- Hoque, M.A.-A., Phinn, S., Roelfsema, C., Childs, I., 2018. Assessing tropical cyclone risks using geospatial techniques. *Appl. Geogr.* 98, 22–33. <https://doi.org/10.1016/j.apgeog.2018.07.004>.
- Houze, R.A., 2012. Orographic effects on precipitating clouds. *Rev. Geophys.* 50 <https://doi.org/10.1029/2011RG000365>.
- IMD, 2021. CYCLONE WARNING IN INDIA STANDARD OPERATION PROCEDURE. Ministry of Earth Sciences, Government of India.
- Jena, P., Garg, S., Azad, S., 2020. Performance analysis of IMD high-resolution gridded rainfall ($0.25^\circ \times 0.25^\circ$) and satellite estimates for detecting cloudburst events over the northwest himalayas. *J. Hydrometeorol.* 21, 1549–1569. <https://doi.org/10.1175/JHM-D-19-0287.1>.
- Knutson, T.R., Sirutis, J.J., Zhao, M., Tuleya, R.E., Bender, M., Vecchi, G.A., Villarini, G., Chavas, D., 2015. Global projections of intense tropical cyclone activity for the late twenty-first century from dynamical downscaling of CMIP5/rcp4.5 scenarios. *J. Clim.* 28, 7203–7224. <https://doi.org/10.1175/JCLI-D-15-0129.1>.

- Kossin, J.P., 2018. A global slowdown of tropical-cyclone translation speed. *Nature* 558, 104–107. <https://doi.org/10.1038/s41586-018-0158-3>.
- Lavender, S.L., McBride, J.L., 2021. Global climatology of rainfall rates and lifetime accumulated rainfall in tropical cyclones: influence of cyclone basin, cyclone intensity and cyclone size. *Int. J. Climatol.* 41, E1217–E1235. <https://doi.org/10.1002/joc.6763>.
- Li, Z., Yu, W., Li, T., Murty, V.S.N., Tangang, F., 2013. Bimodal character of cyclone climatology in the Bay of Bengal modulated by monsoon seasonal cycle. *J. Clim.* 26, 1033–1046. <https://doi.org/10.1175/JCLI-D-11-00627.1>.
- Lohmann, D., Nolte-Holube, R., Raschke, E., 1996. A large-scale horizontal routing model to be coupled to land surface parametrization schemes. *Tellus* 48, 708–721. <https://doi.org/10.1034/j.1600-0870.1996.t01-3-00009.x>.
- LOHMANN, D., RASCHKE, E., NIJSSEN, B., Lettenmaier, D.P., 1998. Regional scale hydrology: I. Formulation of the VIC-2L model coupled to a routing model. *Hydrol. Sci. J.* 43, 131–141. <https://doi.org/10.1080/0262669809492107>.
- Macalalad, R.V., Badilla, R.A., Cabrera, O.C., Bagtasa, G., 2021. Hydrological response of the pampanga river basin in the Philippines to intense tropical cyclone rainfall. *J. Hydrometeorol.* 22, 781–794. <https://doi.org/10.1175/JHM-D-20-0184.1>.
- Mahala, B.K., Nayak, B.K., Mohanty, P.K., 2015. Impacts of ENSO and IOD on tropical cyclone activity in the Bay of Bengal. *Nat. Hazards* 75, 1105–1125. <https://doi.org/10.1007/s11069-014-1360-8>.
- Mahto, S.S., Mishra, V., 2019. Does ERA-5 outperform other reanalysis products for hydrologic applications in India? *J. Geophys. Res. Atmos.* 124, 9423–9441. <https://doi.org/10.1029/2019JD031155>.
- Mishra, V., Shah, R., Azhar, S., Shah, H., Modi, P., Kumar, R., 2018. Reconstruction of droughts in India using multiple land-surface models (1951–2015). *Hydrol. Earth Syst. Sci.* 22, 2269–2284. <https://doi.org/10.5194/hess-22-2269-2018>.
- Mohapatra, M., Bandyopadhyay, B.K., Tyagi, A., 2014. Status and plans for operational tropical cyclone forecasting and warning systems in the north Indian ocean region. In: Mohanty, U.C., Mohapatra, M., Singh, O.P., Bandyopadhyay, B.K., Rathore, L.S. (Eds.), *Monitoring and Prediction of Tropical Cyclones in the Indian Ocean and Climate Change*. Springer Netherlands, Dordrecht, pp. 149–168. https://doi.org/10.1007/978-94-007-7720-0_14.
- Muñoz-Sabater, J., Dutra, E., Agustí-Panareda, A., Albergel, C., Arduini, G., Balsamo, G., Boussetta, S., Choulga, M., Harrigan, S., Hersbach, H., Martens, B., Miralles, D.G., Piles, M., Rodríguez-Fernández, N.J., Zsoter, E., Buontempo, C., Thépaut, J.-N., 2021. ERA5-Land: a state-of-the-art global reanalysis dataset for land applications. *Earth Syst. Sci. Data Discuss.* 1–50. <https://doi.org/10.5194/esdd-2021-82>.
- Nash, J.E., Sutcliffe, J.V., 1970. River flow forecasting through conceptual models part I – a discussion of principles. *J. Hydrol.* 10, 282–290. [https://doi.org/10.1016/0022-1694\(70\)90255-6](https://doi.org/10.1016/0022-1694(70)90255-6).
- National Disaster Management Authority, 2008. National Disaster Management Guidelines. Government of India.**
- Needham, H.F., Keim, B.D., Sathiraj, D., 2015. A review of tropical cyclone-generated storm surges: global data sources, observations, and impacts: a Review of Tropical Storm Surges. *Rev. Geophys.* 53, 545–591. <https://doi.org/10.1002/2014RG000477>.
- Neetu, S., Lengaigne, M., Vialard, J., Samson, G., Masson, S., Krishnamohan, K.S., Suresh, I., 2019. Premonsoon/Postmonsoon Bay of Bengal tropical cyclones intensity: role of air-sea coupling and large-scale background state. *Geophys. Res. Lett.* 46, 2149–2157. <https://doi.org/10.1029/2018GL081132>.
- Nijssen, B., Lettenmaier, D.P., Liang, X., Wetzel, S.W., Wood, E.F., 1997. Streamflow simulation for continental-scale river basins. *Water Resour. Res.* 33, 711–724. <https://doi.org/10.1029/96WR03517>.
- Pai, D.S., Sridhar, L., Rajeevan, M., Sreejith, O.P., Satbhai, N.S., Mukhopadhyay, B., 2014. Development of a New High Spatial Resolution ($0.25^\circ \times 0.25^\circ$) Long Period (1901–2010) Daily Gridded Rainfall Data Set over India and its Comparison with Existing Data Sets over the Region 18.
- Paliwal, M., Patwardhan, A., 2013. Identification of clusters in tropical cyclone tracks of North Indian Ocean. *Nat. Hazards* 68, 645–656. <https://doi.org/10.1007/s11069-013-0641-y>.
- Parida, B.R., Behera, S.N., Oinam, B., Patel, N.R., Sahoo, R.N., 2018. Investigating the effects of episodic Super-cyclone 1999 and Phailin 2013 on hydro-meteorological parameters and agriculture: an application of remote sensing. *Remote Sens. Appl.: Soc. Environ.* 10, 128–137. <https://doi.org/10.1016/j.rsase.2018.03.010>.
- Paschalis, A., Fatichi, S., Molnar, P., Rimkus, S., Burlando, P., 2014. On the effects of small scale space-time variability of rainfall on basin flood response. *J. Hydrol.* 514, 313–327. <https://doi.org/10.1016/j.jhydrol.2014.04.014>.
- Patricola, C.M., Wehner, M.F., 2018. Anthropogenic influences on major tropical cyclone events. *Nature* 563, 339–346. <https://doi.org/10.1038/s41586-018-0673-2>.
- Rao, A.D., Chittibabu, P., Murty, T.S., Dube, S.K., Mohanty, U.C., 2007. Vulnerability from storm surges and cyclone wind fields on the coast of Andhra Pradesh, India. *Nat. Hazards* 41, 515–529. <https://doi.org/10.1007/s11069-006-9047-4>.
- Rao, A.D., Poulose, J., Upadhyay, P., Mohanty, S., 2015. Local-scale Assessment of tropical cyclone induced storm surge inundation over the coastal zones of India in probabilistic climate risk scenario. In: Ravela, S., Sandu, A. (Eds.), *Dynamic Data-Driven Environmental Systems Science*, Lecture Notes in Computer Science. Springer International Publishing, Cham, pp. 79–88. https://doi.org/10.1007/978-3-319-25138-7_8.
- Risser, M.D., Wehner, M.F., 2017. Attributable human-induced changes in the likelihood and magnitude of the observed extreme precipitation during hurricane harvey. *Geophys. Res. Lett.* 44 (12) <https://doi.org/10.1002/2017GL075888>, 457–12,464.
- Rogers, R., Marks, F., Marchok, T., 2009. Tropical cyclone rainfall. In: Anderson, M.G., McDonnell, J.J. (Eds.), *Encyclopedia of Hydrological Sciences*. John Wiley & Sons, Ltd, Chichester, UK, p. hsa030. <https://doi.org/10.1002/0470848944.hsa030>.
- RSMC, 2020. REPORT on CYCLONIC DISTURBANCES over NORTH INDIAN OCEAN during 2019, Annual RSMC Report. INDIA METEOROLOGICAL DEPARTMENT, New Delhi.
- RSMC, 2019. REPORT on CYCLONIC DISTURBANCES over NORTH INDIAN OCEAN during 2018, Annual RSMC Report. INDIA METEOROLOGICAL DEPARTMENT, New Delhi.
- RSMC, 2016. REPORT on CYCLONIC DISTURBANCES over NORTH INDIAN OCEAN during 2015, Annual RSMC Report. INDIA METEOROLOGICAL DEPARTMENT, New Delhi.
- RSMC, 2014. REPORT on CYCLONIC DISTURBANCES over NORTH INDIAN OCEAN during 2013, Annual RSMC Report. INDIA METEOROLOGICAL DEPARTMENT, New Delhi.
- RSMC, 2006. REPORT on CYCLONIC DISTURBANCES over NORTH INDIAN OCEAN during 2005, Annual RSMC Report. INDIA METEOROLOGICAL DEPARTMENT, New Delhi.
- RSMC, 2000. REPORT on CYCLONIC DISTURBANCES over NORTH INDIAN OCEAN during 1999, Annual RSMC Report. INDIA METEOROLOGICAL DEPARTMENT, New Delhi.
- Sahoo, B., Bhaskaran, P.K., 2018. Multi-hazard risk assessment of coastal vulnerability from tropical cyclones – a GIS based approach for the Odisha coast. *J. Environ. Manag.* 206, 1166–1178. <https://doi.org/10.1016/j.jenvman.2017.10.075>.
- Sahoo, B., Bhaskaran, P.K., 2015. Synthesis of tropical cyclone tracks in a risk evaluation perspective for the east coast of India. *Aquatic Procedia* 4, 389–396. <https://doi.org/10.1016/j.aqpro.2015.02.052>.
- Shepard, D., 1968. A two-dimensional interpolation function for irregularly-spaced data. In: Proceedings of the 1968 23rd ACM National Conference on -. Presented at the the 1968 23rd ACM National Conference. ACM Press, Not Known, pp. 517–524. <https://doi.org/10.1145/800186.810616>.
- Singh, O.P., Ali Khan, T.M., Rahman, MdS., 2000. Changes in the frequency of tropical cyclones over the North Indian Ocean. *Meteorol. Atmos. Phys.* 75, 11–20. <https://doi.org/10.1007/s00300700011>.
- Smith, J.A., Baeck, M.L., Meierdiercks, K.L., Nelson, P.A., Miller, A.J., Holland, E.J., 2005. Field studies of the storm event hydrologic response in an urbanizing watershed: field studies OF urban hydrologic response. *Water Resour. Res.* 41 <https://doi.org/10.1029/2004WR003712>.
- Srinivas, C.V., Rao, D.V.B., Yesubabu, V., Baskaran, R., Venkatraman, B., 2013. Tropical cyclone predictions over the Bay of Bengal using the high-resolution advanced research weather research and forecasting (ARW) model. *Q. J. R. Meteorol. Soc.* 139, 1810–1825. <https://doi.org/10.1002/qj.2064>.
- Su, F., Adam, J.C., Bowling, L.C., Lettenmaier, D.P., 2005. Streamflow simulations of the terrestrial Arctic domain. *J. Geophys. Res. Atmos.* 110 <https://doi.org/10.1029/2004JD005518>.
- Titley, H.A., Cloke, H.L., Harrigan, S., Pappenberger, F., Prudhomme, C., Robbins, J.C., Stephens, E.M., Zsoter, E., 2021. Key factors influencing the severity of fluvial flood hazard from tropical cyclones. *J. Hydrometeorol.* <https://doi.org/10.1175/JHM-D-20-0250.1>.
- Villarini, G., Goska, R., Smith, J.A., Vecchi, G.A., 2014. North atlantic tropical cyclones and U.S. Flooding. *Bull. Am. Meteorol. Soc.* 95, 1381–1388. <https://doi.org/10.1175/BAMS-D-13-00060.1>.
- WMO, 2020. Tropical Cyclones [WWW Document]. World Meteorological Organization. URL: <https://public.wmo.int/en/our-mandate/focus-areas/natural-hazards-and-disaster-risk-reduction/tropical-cyclones>.
- Woods, R., Sivapalan, M., 1999. A synthesis of space-time variability in storm response: rainfall, runoff generation, and routing. *Water Resour. Res.* 35, 2469–2485. <https://doi.org/10.1029/1999WR900014>.
- Xing, W., Huang, F., 2013. Influence of summer monsoon on asymmetric bimodal pattern of tropical cyclogenesis frequency over the Bay of Bengal. *J. Ocean Univ. China* 12, 279–286. <https://doi.org/10.1007/s11802-013-2219-4>.
- Zscheischler, J., Martius, O., Westra, S., Bevacqua, E., Raymond, C., Horton, R.M., van den Hurk, B., AghaKouchak, A., Jézéquel, A., Mahecha, M.D., Maraun, D., Ramos, A. M., Ridder, N.N., Thiery, W., Vignotto, E., 2020. A typology of compound weather and climate events. *Nat. Rev. Earth Environ.* 1, 333–347. <https://doi.org/10.1038/s43017-020-0060-z>.